View metadata, citation and similar papers at core.ac.uk

brought to you by CORE

provided by DSpace@MIT

HATSOPOULOS MICROFLUIDS LABORATORY

Department of Mechanical Engineering, Massachusetts Institute of Technology

Elongational Viscosity of Monodisperse and Bidisperse Polystyrene Melts

Jens K. Nielsen, Henrik K. Rasmussen, Ole Hassager, and Gareth H. McKinley

March 2006
HML Report Number 06-P-06

HML@MIT
http://web.mit.edu/fluids

Elongational viscosity of monodisperse and bidisperse polystyrene melts

Jens Kromann Nielsen [1],Henrik Koblitz Rasmussen [2] and Ole Hassager [1]
The Danish Polymer Centre
Department of Chemical Engineering [1]
Department of Manufacturing Engineering and Management [2]
Technical University of Denmark
DK-2800 Kgs. Lyngby, Denmark

Gareth H. McKinley
Hatsopoulos Microfluids Laboratory
Department of Mechanical Engineering
Massachusetts Institute of Technology
Cambridge, Massachusetts 02139, USA

Abstract

The startup and steady uniaxial elongational viscosity have been measured for two monodisperse polystyrene melts with molecular weights of $52\,^{\mathrm{kg}}/_{\mathrm{mole}}$ and $103\,^{\mathrm{kg}}/_{\mathrm{mole}}$, and for three bidisperse polystyrene melts. The monodisperse melts show a maximum in the steady elongational viscosity vs. the elongational rate, $\dot{\epsilon}$, of about two times $3\eta_0$ whereas the bidisperse melts have a maximum of up to a factor of 7 times the Trouton limit of $3\eta_0$. The Wiest model which incorporates anisotropic drag and finite extensibility may be used to interpret the results in molecular terms.

1 Introduction

The scaling of linear viscoelastic properties such as the zero shear viscosity, η_0 and the characteristic reptation time , τ_d, for the Doi-Edwards model (Doi and Edwards, 1986) have been investigated thoroughly both theoretically and experimentally in the literature for monodisperse polymer melts. It is commonly accepted that the zero shear viscosity and the reptation time both scale with the molecular weight as $\eta_0 \sim M^{3.4}$ and $\tau_d \sim M^{3.4}$ for monodisperse polymers with molecular weights substantially above the entanglement molecular weight, $M > (2-4)M_e$. Elongational flow properties have however not been analyzed as intensely. Thorough investigation of the elongational viscosity for very diluted solutions of monodisperse (and bidisperse) polystyrene have been made and analyzed by Gupta et al. (2000) and Ye et al. (2003). Wagner et al. (2005) have recently published elongational results for bidisperse blends of small amounts of ultra high, narrow molecular weight polystyrene ,$M_w = 3220\,\mathrm{Kg/mole}$ and $M_w = 15400\,\mathrm{Kg/mole}$ in lower molecular weight polydisperse polystyrene, $M_w = 423\,\mathrm{Kg/mole}$. Steady state was never reached, but the authors found that the blends were more strain hardening than the monodisperse melts, and that maximum amount of strain hardening increased with increasing content of ultra high molecular weight polystyrene. To our knowledge the only published steady elongational viscosities for monodisperse melts are those of Bach et al. (2003a) and Luap et al. (2005). Neither the Doi-Edwards model nor other reptation-based models (Marrucci and Grizzutti (1988), Mead et al. (1998), Fang et al. (2000), Ianniruberto and Marrucci (2001), Schieber et al. (2003)) have effectively been able to predict the flow behaviour of especially high Deborah-number flows, i.e. fast elongational flows with $\dot{\epsilon} \geq 1/\tau_d$. Indeed, the major limitation to progress in the understanding of the nonlinear properties in elongational flow seems to be the scarcity of data for well-characterized narrow molecular weight linear polymer melts.

There have been a number of recent efforts at extending the basic reptation picture to incorporate additional physical mechanisms that modify the evolution in the polymeric stress in strong stretching flows. These include incorporating the role of 'intrachain pressure' within a differential framework (Marrucci et al. 2004) and within the integral molecular stress function formulation (Wagner et al. 2005) or through detailed analysis of the rate of creation and destruction of 'slip links' (Likhtman 2005). The key change that each of these models seek to incorporate is a modification in the scaling of the steady elongational steady stress with the elongational rate, $\sigma_{zz} - \sigma_{rr} \sim \dot{\epsilon}^n$. The bare reptation model of Doi and Edwards predicts a saturation in the stress, $n = 0$ (corresponding to thinning in the elongational viscosity). Incorporation of chain stretching results in unbounded stress growth, which can be truncated through considering the finite extensibility of the chains resulting ultimately in $n = 1$ (Fang et al. 2000) corresponding to finite limiting value of the elongational viscosity. The proposed models by Marrucci and Ianniruberto (2004) and Wagner et al. (2005) both find that $n = 0.5$. In the present work we use the simple model proposed by Wiest (1989) which models the effects of the surroundings chains as an anisotropic drag acting on a finitely-extensible dumbbell that represents a single segment of the orienting and elongating chain. This computationally simple model gives $n = 0.5$ and we show below that it is able to capture many of the important features that we observe in the steady elongational viscosity.

Bach et al. (2003a) measured the elongational viscosity of two narrow molar mass distribution polystyrene melts, with $M_w = 200\,\mathrm{kg/mole}$, PS200K, and $M_w = 390\,\mathrm{kg/mole}$, PS390K. The main conclusions drawn from this work were: 1) The steady elongational viscosity for Deborah numbers, defined as $De = \dot{\epsilon}\tau_d$ greater than unity scales as $\bar{\eta} \sim \dot{\epsilon}^{-0.5}$. 2) The steady elongational viscosity scales linearly with the molecular weight for $De > 1$, i.e. $\bar{\eta} \sim M_w\dot{\epsilon}^{-0.5}$ and finally 3) the steady elongational viscosity is a monotone decreasing function of the elongational rate. That is, $\bar{\eta}$ does not exceed $3\eta_0$ for any elongational rate accessed experimentally. The authors did point out,

that their conclusions with regard to molecular mass scaling were based on merely two samples. Based on the scaling properties of η_0 and τ_d with the molecular weight it is however realized that these conclusions cannot be true if one extends them to elongational measurements of lower molecular weights. There are simply too many constraints. Marrucci and Ianniruberto (2004) have treated this problem theoretically and suggested that melts with fewer entanglements may show a maximum in $\bar{\eta}$ as function of $\dot{\epsilon}$.

The first purpose of this work is to investigate how two polystyrene melts with $M_w = 103\,{}^{\mathrm{kg}}/_{\mathrm{mole}}$, PS100K, and $M_w = 52\,{}^{\mathrm{kg}}/_{\mathrm{mole}}$, PS50K, behave in a uniaxial elongational flow at 130°C. Polystyrene has an entanglement molecular weight of $M_e = 13.3{}^{\mathrm{kg}}/_{\mathrm{mole}}$ (Fetters et al., 1994), giving the melts respectively 7.7 and 3.9 entanglements. With these fluids it is possible to analyze what happens to $\bar{\eta}$ in the transition going from low to high Deborah numbers, i.e. from the linear to the non-linearly dominated regime. The elongational measurements can give an indication of which of the constraints noted above must be relaxed.

The reptation time for PS100K is $\tau_d \approx 100s$ at $130°C$. The range over which the elongational rates can be measured by the filament stretching rheometer (FSR) to avoid dissipative heating in the sample is $\dot{\epsilon} \leq 0.3s^{-1}$ (Bach et al. 2003a), making it possible to transition from low to high Deborah numbers for PS100K. The lower molecular weight PS50K sample is expected mostly to provide information about the linear region, since $\tau_d \approx 10s$.

The lack of a maximum in $\bar{\eta}$ vs. $\dot{\epsilon}$ for PS200K and PS390K is believed to be related to the monodisperse character of the melts, and it has therefore been decided to make three bidisperse melts, in which each of the individual polymers in the blend are expected not to display a maximum in $\bar{\eta}$ vs. $\dot{\epsilon}$ when studied in isolation. We have decided to mix PS390K with PS50K in two different concentrations in order to investigate the effect of diluting PS390K with PS50K. Secondly we have made a mixture of PS390K with PS100K, where PS390K has the same mass-concentration as one of the PS390K+PS50K-blends.

The composition of the three blends used in the work is shown in table 1. In this table we also show the concentration of PS390K relative to the overlap concentration, c*, of PS390K in a dilute solution under theta conditions defined by Doi (1992) (page 20). The radius of gyration R_g for PS390K is found to be $R_g = 168nm$, (Fetters et al., 1994), and since one polymer has a volume of order $O(R_g^3)$, the overlap concentration of PS390K is found to be c*=$16kg/m^3$, or c*=$1.6w/w\%$. We also specify in table 1 the weight-average molecular weight of the bi-disperse blends, $M_w = \phi_L M_L + \phi_S M_S$ where ϕ_i and M_i are the weight fractions- and the molecular weights of the long chain (L) and short chain (S) components.

2 Experimental section

2.1 Synthesis and Chromatography

The two polystyrene samples PS50K and PS100K were synthesized by anionic polymerisation (Ndoni et al. 1995). The molecular weights were determined by size exclusion chromatography (SEC) with toluene as the eluent using a Viscotec 200 instrument equipped with a PLguard and two PLgel mixed D columns in series (from Polymer Laboratories) using a RI detector. On the basis of calibration with narrow molecular weight polystyrene standards, the values of M_w and M_w/M_n were measured for the monodisperse samples. The results are given in table 2.

2.2 Mechanical Spectroscopy

The viscoelastic properties of the polystyrene melts were obtained from small amplitude oscillatory shear flow measurements on an AR2000 rheometer from TA instruments using a plate-plate ge-

ometry (see figure 1 and 2). The measurements were performed at 130°C for the PS50K, PS100K and blends, and at 150°C for the blends. The measured data at 150°C was shifted to 130°C using the time temperature superposition shift factor a_T found from the WLF-equation (Bach et al. 2003a):

$$log_{10}(a_T) = \frac{-c_1^0(T - T_0)}{c_2^0 + (T - T_0)} \tag{1}$$

where $c_1^0 = 8.86$, $c_2^0 = 101.6°C$, $T_0 = 136.5°C$ and T is the sample temperature in °C.

2.3 Transient elongational viscosity measurements

The transient elongational viscosity was measured using a filament stretching rheometer which is described in detail elsewhere (Bach et al. 2003b). The polystyrene melts were dried according to the protocol of Schausberger and Schindlauer (1985), and moulded into cylindrical-shaped samples, with radius of $R_i = 4.5mm$ and height of $L_i = 2.5mm$ using a Carver hydraulic press. The PS50K and PS100K-samples were pressed at 150°C and annealed at this temperature for 2 minutes. The bidisperse blends were pressed and annealed for 2 minutes at 170°C. The temperatures were chosen to ensure that the polymer chains were completely relaxed and still did not degrade; this was confirmed using SEC after the elongational experiment was performed. The moulded pellets were placed between two parallel plates inside the filament stretching rheometer, and the temperature was raised to 130°C. To ensure adhesion between the end plates and polymer melt, the end plates were coated with a solution of polystyrene in tetrahydrofuran as described in Bach et al. (2003a). In most of the experiments performed the sample was pre-stretched in order to reduce the transmitted force in the vertical plane to avoid the sample being ripped of the end plates. All samples was pre-stretched by variable amounts, thus the initial radius for experiments with PS100K at $\dot{\epsilon} = 0.3s^{-1}$ was $R_0 = 1.5mm$, whereas the initial radius for Blend 3 was $R_0 = 4.3mm$ at $\dot{\epsilon} = 0.00015s^{-1}$. The pre-stretch was performed with stretch rates considerably lower than the inverse of the longest relaxational time. The melt is allowed to relax before every elongational experiment is started. We wait until all residual orientation in the polymer has disappeared, which is the case when no residual forces are present as indicated by the load cell. This equilibration time is at least ten times the longest relaxation time of the melt.

During a stretching experiment a laser micrometer samples the central diameter of the elongating filament while a load cell measures the force at the end plate. The diameter data is sent directly to a controller that produces a signal to the motor pulling the end plates apart. This control method ensures that the radius decreases exponentially with time as $R(t) = R_0 e^{-\dot{\epsilon}t/2}$. The Hencky strain is defined as $\epsilon = -2\ln(R(t)/R_0)$. After an elongational experiment is complete, the measured radius $R(t)$ and force $F(t)$ are used to calculate the tensile stress

$$\sigma_{zz} - \sigma_{rr} = \frac{F(t) - m_1 g}{\pi R(t)^2} \tag{2}$$

and the transient elongational viscosity as:

$$\bar{\eta}^+(t) = \frac{\sigma_{zz} - \sigma_{rr}}{\dot{\epsilon}} \tag{3}$$

where the measured force, F, is corrected by the weight of lower half of the polymer filament, m_1 and the gravitational acceleration g (Szabo 1997). This weight is measured by forcing the filament to break at the symmetry plane after the end of an experiment.

At small strains there is an extra force contribution from the shear components in the deformation field during start-up. The shear component originates from the no slip condition at the rigid end plates and is especially important at small aspect ratios. For Newtonian fluids this reverse

squeeze flow problem can be modelled analytically and the effect of the additional shear may be eliminated by a correction factor (Spiegelberg and McKinley (1996)).

$$\bar{\eta}^{+}_{corr} = \bar{\eta}^{+} \left(1 + \frac{\exp(-7\epsilon + \epsilon_0)/3)}{3\Lambda_i^2} \right)^{-1} \tag{4}$$

where $\Lambda_i = L_i/R_i$ is the initial aspect ratio, ϵ_0 is the pre stretched Hencky strain, defined as $\epsilon_0 = -2\ln(R_0/R_i)$ and $\bar{\eta}^{+}_{corr}$ is the corrected transient uni-axial elongation viscosity.

This correction is analytically correct for very small strains ($\epsilon \to 0$) for all types of fluids. However, the correction is less accurate at increasing strains where the effect of the correction fortunately vanishes.

In this work we have chosen to present the elongation measurements in both uncorrected and corrected form, as we also prefer to present the raw data. For the aspect ratio used here, the extra force contribution is negligible after about one additional strain unit . This was demonstrated experimentally in Bach et al. (2003b), and theoretically in Kolte et. al. (1997) for polymer melts.

Eriksson and Rasmussen (2005) suggest that the relevant non-dimensional measure of the surface tension in viscoelastic flow is the ratio of the surface tension stresses to the complex modulus $G^*(\omega) = \sqrt{G'(\omega)^2 + G''(\omega)^2}$, i.e. Vc= $\sigma/(RG^*(\dot{\epsilon}))$, where the angular frequency, ω, has been replaced with the characteristic deformation rate, $\dot{\epsilon}$. This Viscoelastic Capillary number resembles the surface elasticity number, (Spiegelberg and McKinley (1996) and Rasmussen and Hassager (2001)) at high deformation rates and the inverse of the classical Capillary number at low deformation rates. As Vc stays below 0.03 in all experiments, the effect of surface tension is negligible.

The effect of gravitational sagging can be evaluated using a relevant measure of the magnitude of gravitational forces relative to the viscous forces. Here we use the ratio $L_i \exp(\epsilon + \epsilon_0)\, \rho g/(2\dot{\epsilon}\bar{\eta}^{+})$ as in Rasmussen et al. (2005) where ρ is the density of the polymer melt. The duration of the elongational experiments in this work were considerably below the sagging time, as this number is less than 0.1 in all the performed experiments.

See Szabo and McKinley (2003) for additional discussion of similar correction factors.

3 Linear Viscoelastic Measurements

A linear viscoelastic (LVE) analysis provides us with an estimate of the elongational behaviour in the limit $De \to 0$ and provides a verification of the reliability of the elongational experiments especially at short times and small strains. If the verifications of the experiments were the sole purpose of doing LVE-experiments a simple Maxwell-fit to the data would be sufficient. But we also seek to determine the characteristic time constants of the individual polymeric species in the melt, and for this the Baumgaertel, Schausberger and Winter (BSW) model is used (Baumgaertel et al. 1990). Each polymer contributes a distinct spectrum with a characteristic time constant. We analyse the LVE-data with a theoretical approach suggested by Jackson and Winter (1995) which handles mono- and bidisperse melts. This is not to be confused with a blend rule, since the LVE-properties of the blends cannot be predicted from the composition of long- and short polymers by this procedure. The LVE properties of monodisperse linear polymers (Milner and McLeish, 1998) and mixing rules for blends of monodisperse species (des Cloizeaux (1988)) have been studied in detail. In terms of physical insight the BSW-approach is not far from a simple Maxwell-fit, with few exceptions as described later.

The relaxation modulus $G(t)$ is found from the continuous-spectrum $H(\lambda)$, which for the bidisperse blends is composed of two individual spectra:

$$G(t) = G_1(t) + G_2(t) \tag{5}$$

$$G_i(t) = \int_0^\infty \frac{H_i(\lambda)}{\lambda} \exp(-t/\lambda) d\lambda, \quad i = 1, 2 \tag{6}$$

$$H_i(\lambda) = n_e G^0_{N,i} \left[\left(\frac{\lambda}{\lambda_{max,i}} \right)^{n_e} + \left(\frac{\lambda}{\lambda_c} \right)^{-n_g} \right] h(1 - \lambda/\lambda_{max,i}) \tag{7}$$

Here $h(x)$ is the Heaviside step function, n_e is the slope of the $(log(\omega), logG')$ curve at intermediate frequencies ω, n_g is the slope of $(\log(\omega), \log G'')$ for $\omega \to \infty$, and λ_c is called the crossover relaxation time. We constrain the individual contributions to the modulus in a way such that $G^0_N = G^0_{N,1} + G^0_{N,2}$ is constant.

When least-squares fitting (Rasmussen et al. 2000) the BSW model to the LVE data, n_e, n_g (both independent of temperature), λ_c and G^0_N are treated as fixed values. The cross over time λ_c depends on temperature as any other relaxation time. $n_e = 0.23$, $n_g = 0.67$ and $\lambda_c = 0.4s$ (at $130°C$) as obtained by Jackson and Winter (1995). The value of G^0_N was found by Bach et al. (2003a) to be 250 kPa at 130°C, and we have decided to use this value as a fixed parameter. This means, that the only remaining adjustable parameters to model the LVE data are the two largest relaxation times, $\lambda_{max,1}$ and $\lambda_{max,2}$ as seen in table 3.

Since the monodisperse melts only have one largest time constant λ_{max}, this is the single adjustable parameter for fitting the LVE data for PS50K, PS100K and PS390K to the BSW-model. In order to be able to compare the properties of monodisperse and bidisperse melts, the same values of n_e, n_g and λ_c are always used. The model parameters are given in table 3, obtained by least squares fitting the measured values of G' and G''. The experimental results for G' and G'' are shown in figures **??** and **??** together with the best fit of the BSW-model. The zero shear viscosities are calculated as:

$$\eta_{0,i} = \int_0^\infty G_i(s) ds = n_e G^0_{N,i} \lambda_{max,i} \left(\frac{1}{1+n_e} + \frac{1}{1-n_g} \left(\frac{\lambda_{max,i}}{\lambda_c} \right)^{-n_g} \right) \tag{8}$$

For the monodisperse melts $i = 1$. For the bidisperse melts $i = 1, 2$, and the individual $\eta_{0,i}$ can be added to find the actual, measured value of $\eta_0 = \eta_{0,1} + \eta_{0,2}$.

Fitting η_0 for the monodisperse melts PS50K, PS100K, PS200K and PS390K with the molecular weight as a power law, the exponent is found to be 3.38 as generally observed for these moderately entangled systems.

The average reptation time is calculated as:

$$\lambda_{a,i} = \frac{\int_0^\infty G_i(s) s ds}{\int_0^\infty G_i(s) ds} \approx \lambda_{max,i} \left(\frac{1+n_e}{2+n_e} \right) \tag{9}$$

This expression applied to the Doi Edwards relaxation modulus gives a value that is within 2% of the commonly denoted reptation time, τ_d. This time is found to scale with molecular weight as $\lambda_a \sim M^{3.52}$ for our monodisperse melts.

The characteristic time constants for the bidisperse systems found in Table 3 show that the smaller time constant in the blend is more or less unchanged compared to the time constant for the undiluted small molecular weight melt. This is in agreement with the expectation (Doi et al. 1987) that there will be no tube dilation for the short chains. By contrast the longest relaxation time in the blend has been significantly reduced compared to the longest relaxation time for an undiluted melt of long chains which is attributed to the effect of tube dilation, Doi et al. (1987).

Struglinski and Graessley (1985) have predicted that when the molar masses in a binary blend of short (M_s) and long (M_l) chains are far apart, the reptation time for the longest molecules should not depend on the blend composition. The relevant constraint release parameter is defined as $G_r = M_L M_e^2 / M_S^3$ with the prediction that the reptation time of the longer chains should be unchanged provided $G_r < 0.1$. More recent investigations (Lee et al. 2005 and Park et al. 2004), however, suggest that the critical condition is somewhat lower with $G_{rc} \approx 0.064$ such that the non-dilation regime is limited to $G_r < G_{rc}$. The constraint release parameters for our blends (shown in Table 1) are indeed all larger than G_{rc} indicating that tube dilation takes place and that relaxation of the stress carried by the long chains is the result of constraint release due to reptation of the short chains. This is reflected in the values of $\lambda_{a,2}$ for the blends compared to the value $\lambda_{a,1}$ for the pure long chains (PS390K) in table 3. By contrast the short relaxation time of blend ($\lambda_{a,1}$) is substantially unchanged compared to that of the pure short chains indicating that the short chains are reptating in an essentially frozen network of long chains. Moreover according to the revised Struglinski and Graessley criterion our blend 3 should be the least affected by tube dilation also in agreement with observations.

Struglinski and Graessley also conclude that the zero shear viscosity η_0 for bidisperse melts depends on the weight average molecular weights as the monodisperse melts where $\eta_0 \sim M_w^{3.4}$. This prediction deviates less than 40 percent from our measured zero shear viscosities.

Ye et al. (2003) used two monodisperse polystyrene samples of molar masses $M_s = 2890\,{}^{\mathrm{kg}}/_{\mathrm{mole}}$ and $M_l = 8420\,{}^{\mathrm{kg}}/_{\mathrm{mole}}$ to prepare a series of bidisperse solutions spanning the range from pure short chains to long chains. All blends were dissolved in tricresyl phosphate with an overall polymer volume fraction of 7%. These blends, all in the semidilute regime, were subsequently characterized in uniaxial extensional flow and successfully compared to the predictions of a simplified reptation model designed to investigate the effects of polydispersity. A characteristic feature of the steady elongational viscosity is that all investigated solutions, including the monodisperse solutions show a transition to strain hardening and which is interpreted as a signature of chain stretching. In other words there was no qualitative difference between the measured elongational viscosity of the entangled monodisperse and bidisperse polystyrene solutions. The results obtained by Ye et al. are thus expected to differ from our study for at least two reasons. Firstly, in Table 1 we show the values of the Struglinski-Graessley parameter G_r for the blends studied by Ye et al. The widely disparate values of the reptation times for the two species lead to $G_{rc} << 1$ and indicate that, in contrast to our experiments, the dynamics of the longer chain should remain unchanged regardless of the presence of the shorter species. Secondly, the materials studied by Ye et al. are semi-dilute entangled solutions rather than melts. Even though the number of entanglements is comparable, the higher molecular weight of each entangled segment when diluted by a solvent results in a greater number of Kuhn steps in each segment and consequently a larger molecular extensibility (Appendix 8.2).

4 Elongational Viscosity Measurements

4.1 Startup of elongational flow

Figures **??**, **??** and **??** show the corrected transient elongational viscosity (equation **??**) for PS50K, PS100K, Blend 1 and Blend 3 together with the LVE-prediction, all measured at 130°C. The elongational measurements for all melts show good agreement with the LVE prediction at small

strains. The deviation between the transient elongational data and LVE measurements is less than 15% in all measurements. Figures **??**, **??**, **??** and **??** show the same measurements as in the Figures **??**, **??** and **??**, with uncorrected tensile stress differences (equation **??**) plotted against strain. It is seen, that the steady elongational viscosity is obtained for all elongational rates. As the elongational rate increases, the plateau region is maintained for fewer strain units compared to smaller rates. This is due to a larger pre-stretch, ϵ_0, for the high stretch rate experiments. **The reason for increasing the pre-stretch in the faster experiments is two-fold. Firstly, it minimizes the magnitude of the correction for reverse squeeze flow (see eq.(4)). Secondly it helps reduce the tendency for deadhesion of the sample from the endplate. The adhesive force holding the sample to the end plate has a maximum value; by pre-streching the sample to induce a neck at the midplane, higher tensile stresses (and hence higher maximum stretching rates) can then be tolerated in the middle of the filament for a given force of adhesion at the end-plates.**

4.2 Steady viscosity scaling at intermediate Deborah numbers

4.2.1 Monodisperse melts

We first turn our attention to the results for the monodisperse melts in order to compare with the results from Bachs et al. (2003a). We see from figure **??** and **??** that the steady viscosity for PS100K reaches a value very close to $3\eta_0$ for the lowest elongational rate. The time dependent transient viscosity, $\bar{\eta}^+$, for the lowest rate follows the LVE-prediction. At intermediate Deborah numbers, i.e. $1 < De < 10$, the steady elongational viscosity, $\bar{\eta}$ rises above $3\eta_0$. For PS100K $\bar{\eta}$ is about 50% above $3\eta_0$, and the $\bar{\eta}$-maximum is stretched over two decades of $\dot{\epsilon}$. The maximum for PS50K is measured to be at least 100% above $3\eta_0$. It is possibly higher than $6\eta_0$, since the highest measured elongational rate also gives the highest $\bar{\eta}^+$-value. The rate at which the maximum occurs corresponds to a Deborah number around $De \approx 3$ for both melts (assuming that $\bar{\eta}$ reaches its maximum at a elongational rate somewhat higher than $\dot{\epsilon} = 0.3s^{-1}$ for PS50K).

The elongational viscosity measurements for PS100K and PS50K in the non linear regime, i.e $De > 3$ are very limited because of the restriction due to dissipitative heating limiting the measurements to $\dot{\epsilon} \leq 0.3s^{-1}$. There are only two measurements in the nonlinear regime available for PS100K, and none for PS50K. This makes it difficult to compare with the scaling behaviour proposed by Bach et al. (2003a).

Bach et al. (2003a) claimed that the steady elongational stress scaled linearly with the molecular weight at high Deborah numbers. This scaling can be illustrated by interpretating data according to recently published theory by Marrucci and Ianniruberto (2004). Figure **??** shows steady values of $(\sigma_{zz} - \sigma_{rr})/G_N^0$ vs. $\dot{\epsilon}\tau_p$ for all of the monodisperse melts. Here τ_p represents the relaxation time of the squeezing pressure effect as defined by Marrucci and Ianniruberto (2004). Marrucci and Ianniruberto report τ_p for PS200 to be $\tau_p = 1000s$, and the scaling is $\tau_p \sim M_w^2$. This is used to calculate τ_p for the other monodisperse melts, which then become: $\tau_p = 66.8s$ for PS50K, $\tau_p = 264.2s$ for PS100K and $\tau_p = 3802.5s$ for PS390K. It is seen in figure **??**, that the scaled values for PS50K and PS100K lie on the same line as the data for PS200K and PS390K steady state stresses, hereby showing that the linear scaling of steady stress with molecular weight at high Deborah-numbers is valid.

Another conclusion from the work of Bach et al. (2003a) was that the steady elongational viscosity scales with about $\dot{\epsilon}^{-0.5}$ for large Deborah numbers. By examining the raw-data from Bach et al. (2003a) more closely and performing a linear regression it is however concluded that the exponent is -0.42 ± 0.03 within a 95% confidence interval. In the present study there are only two measurements of $\bar{\eta}$ for PS100K that could confirm this power law behaviour, and none

for PS50K. Figure **??** shows the steady elongational viscosity of PS100K, and it appears to show the expected asymptotic behaviour.

4.2.2 Bidisperse melts

Figure **??** and **??** show the corrected transient elongational viscosity for the blends denoted Blend 1 and Blend 3, see Table 1. It can be seen from both plots, that there is good agreement between the elongational measurements and the LVE prediction for small strains. The steady viscosity lie substantially above $3\eta_0$ for all measurements, except for Blend 3 at $\dot{\epsilon} = 0.3s^{-1}$.

The complex interdependence of the transient extensional rheology of entangled blends on stretching rate, molecular weight and concentration is illustrated in Figure 11 for the PS50K/PS390K blends. For a pure 50K melt at a strain rate of $\dot{\epsilon} = 0.1s^{-1}$ the transient extensional response closely follows the linear viscoelastic envelope. The addition of a small concentration of high molecular weight to the blend (Blend 1; c/c* = 2.5) results in a substantial transient strain-hardening and also a steady extensional viscosity that is substantially above $3\eta_0$ for the blend. That this additional stress is contributed by the higher molecular species can be easily demonstrated by examining the tensile stress contribution associated with a single mode Upper Convected Maxwell, (UCM) model (with modulus and relaxation time determined from Table 3). This is shown by the dashed line in Figure ??. As the concentration of higher molecular weight species is increased to 14% (Blend 2) the magnitude of the extensional viscosity climbs further. Once again we show the contribution of the high molecular weight species to the transient stress growth by plotting the response of an UCM model (solid line). The increase in the relaxation time of blend 2 also results in an increase in the Deborah number ($De_{blend2} = 1755s \cdot 0.1s^{-1} = 176$) and consequently the chains are fully elongated during the course of the experiment. This is illustrated by the horizontal dotted line in Figure 11 which corresponds to cutting off the stress growth for Blend 2 at a Hencky strain of $\epsilon_{max} = \frac{1}{2}ln(N_{K,seg}) = 1.55s^{-1}$, see appendix 8.2. Although the ultimate steady elongational viscosity shows some increase over 3 times the steady shear viscosity for this blend, it is clearly reduced substantially compared to Blend 1. Finally we also show in Figure 11 the transient response of the pure PS390K material at the same imposed stretch rate of $0.1s^{-1}$, together with the UCM model (dashed dot line). The material shows an initial linear viscoelastic response, followed by strain-hardening but a steady elongational viscosity that is substantially less than $3(\eta_0)$.

Plotting the steady elongational viscosity against elongational rate in figure **??**, **??** and **??** , it is seen that the maximum in elongational viscosity is about 90% above $3\eta_0$ for Blend 3, and about 700% above for Blend 2.

5 Constitutive Modelling of the Steady Elongational Viscosity

The mathematical inconsistency mentioned in the introduction is solved by acknowledging that the steady elongational viscosity for moderately entangled melts can have a maximum that exceeds $3\eta_0$; the magnitude of the maximum depending on the molecular weight. The viscosity was found to scale with $\dot{\epsilon}^{-0.4}$ for large Deborah numbers, but where Bach et al. (2003a) claimed that this behaviour starts at $De > 1$, the results from PS100K show that this occurs at much higher Deborah numbers, $De > 10$, and for PS50K even higher. It is thus clear that the shape of the

steady elongational viscosity curve $\bar{\eta}$ is molecular weight dependent. The results from the blends show, that the magnitude of the steady viscosity maximum becomes greater as the difference between the chain lengths in the blend increase.

The behaviour of the elongational viscosity for dilute solutions for high Deborah numbers has been studied by Gupta et al. (2000) who found that $\bar{\eta} \sim \dot{\epsilon}^{-0.5}$ for very diluted solutions of narrow molar mass distribution polystyrene. This result can be modeled theoretically by including finite extensibility into the Giesekus (1982) anisotropic friction dumbbell model to account in an average fashion for the orientation of the surrounding molecules (Wiest 1989). The asymptotic analysis is performed in details in the Appendix.

Marrucci and Ianniruberto (2004) quantitatively predict the experimentally found asymptotic stress behaviour by incorporating chain squeeze into their model. This will essentially give rise to anisotropic friction too, and the Wiest model is a simple way of describing this.

The constitutive model in terms of integral average of the connector dyad $\langle \mathbf{QQ} \rangle$ is:

$$\langle \mathbf{QQ} \rangle_{(1)} = -\frac{4H}{\boldsymbol{\zeta^{-1}}} \left(f\langle \mathbf{QQ} \rangle - \frac{kT}{H}\boldsymbol{I} \right) \tag{10}$$

$$= 4kT\boldsymbol{\zeta^{-1}} - 4H\langle \mathbf{QQ} \rangle f\boldsymbol{\zeta^{-1}} \tag{11}$$

where the Giesekus mobility tensor is:

$$\boldsymbol{\zeta^{-1}} = \frac{1}{\zeta}\left(\boldsymbol{\delta} - \frac{a}{nkT}\boldsymbol{\tau_p} \right) \tag{12}$$

and f describes the nonlinearity of the Warner spring in the FENE-P dumbbell model:

$$f = \left[1 - \frac{\langle Q^2 \rangle}{Q_0^2} \right]^{-1} \tag{13}$$

where $\langle Q^2 \rangle = tr\langle \mathbf{QQ} \rangle$. Here H is a spring constant, n is the number density of dumbbells, k is Boltzmann's constant, T the absolute temperature, $\boldsymbol{I}$ is the unit tensor, and Q_0 is the maximum length of the dumbbell. The stress tensor for the polymer is given by eq. (13.7-5) of Bird et al (1987):

$$\boldsymbol{\tau_p} = -nHf\langle \mathbf{QQ} \rangle + nkT\boldsymbol{\delta} \tag{14}$$

By elimination of $\langle \mathbf{QQ} \rangle$ a constitutive equation in terms of the polymeric stress, $\boldsymbol{\tau_p}$, may be obtained in the form:

$$\left(Z - \lambda_H \frac{DlnZ}{Dt} \right) \boldsymbol{\tau_p} + \lambda_H \boldsymbol{\tau}_{p,(1)} - \frac{aZ}{nkT}(\boldsymbol{\tau_p}\boldsymbol{\tau_p}) = -nkT\lambda_H \left(\dot{\boldsymbol{\gamma}} + \frac{DlnZ}{Dt}\boldsymbol{\delta} \right) \tag{15}$$

Where

$$Z = \frac{1}{b}\left(b + 3 - \frac{tr\boldsymbol{\tau_p}}{nkT} \right) \tag{16}$$

$\dot{\boldsymbol{\gamma}}$ is the strain rate tensor and b is the finite extensibility parameter for the entanglement segment found as: $b = H_{seg}Q_0^2/(kT)$ and λ_H is the single time constant of the model $\lambda_H = \zeta/(4H_{seg})$. The zero shear viscosity is found (Wiest, 1989) to be $\eta_0 = nkT\lambda_H b/(b+3)$.

This model has three free parameters, a, b and λ_H, where a is a dimensionless scalar between 0 and 1 describing the degree of anisotropy in the hydrodynamic drag in the melt; when $a = 0$ the drag is completely isotropic while $a = 1$ corresponds to maximum anisotropy. **The model describes the dynamics of one entanglement. The finite extensibility parameter b is independent of molecular weight and** equal to three times the number of Kuhn steps in a entanglement segment, $N_{k,seg}$, and λ_H is a characteristic time constant. The ratio of the contour length of the molecule to the root mean square end-to-end distance of the equilibrium scales with $\sqrt{N_{k,seg}}$. By solving the constitutive equation for uniaxial elongational flow one sees, that by changing the a-parameter from 0 to 1 at fixed values of b and λ_H, the steady elongational viscosity $\bar{\eta}$ has a maximum above $3\eta_0$, whose magnitude increases as $a \to 0$, and decreases, and almost disappears as $a \to 1$.

Relating the maximum in $\bar{\eta}$ with drag anisotropy for monodisperse melts may help rationalize why the local maximum is almost absent for high molecular weight melts, such as PS390K, and becomes increasingly larger with lower molecular weights. If the size of a is interpreted as a potential for anisotropy, one would intuitively assume that for a 100% stretched and aligned polymer melt, which would be the case at infinite elongational rate at steady state, the anisotropy inside the melt would be largest in the limit of long chains. A melt of shorter, but still stretched and aligned chains, would have a higher density of free ends thereby reducing anisotropy.

The same arguments can be used for bidisperse melts. Blend 1 and 2 contain the same polymers, but the long chains are more diluted by short chains in Blend 1 and we would expect the a-parameter for Blend 2 to be larger than for Blend 1, since the potential for anisotropic drag is lowest when the longer chains are surrounded by fewer long chains. Blend 2 and 3 have the same mass fraction of PS390K, but are mixed with PS50K and PS100K chains, respectively. Again we expect the anisotropic parameter a to be smallest for Blend 2, which is the case as shown later. This effect is more pronounced compared to the difference between Blend 1 and 2.

The question is now whether or not the model is able to explain the data quantitatively. If the model is fitted to results of the monodisperse melts, ideally only two parameters should be fitted, a and λ_H, since b is related to the number of Kuhn steps in an entanglement segment which is known. It is not expected that a single mode version of the model will describe the complete transient elongational viscosity because the initial transient growth in the stress is related to the LVE behaviour, and the Wiest model is basically a single time constant model with inclusion of anisotropy and a FENE-P spring between the dumbbells. A multi mode version would be needed to quantitatively describe the LVE behaviour. Since we are concerned primarily with the steady elongational viscosity only one mode is used in this analysis.

PS100K is the melt with the most elongational measurements above and below $\dot{\epsilon} = 1/\tau_d$, i.e. at intermediate Deborah numbers, which in this work is the most interesting area. To obtain an idea of the relative magnitude of the different constitutive parameters, a fit to the elongational viscosity data for PS100K is made by changing both a b and λ_H, and a separate fit where b is kept constant at $3N_{k,seg}$ and only a and λ_H are allowed to change. Bach et al. (2003a) reported the number of Kuhn steps between entanglement segments as $N_{k,seg} = 22$, which makes $b = 66$. The result is shown in figure **??**, and the fitted values are shown in the caption. Both fits give reasonable agreement with the experimental data. The time constant λ_H is in both fits of about the order of the expected reptation time in both fits, around 100 seconds, and a is in the expected interval between 0 and 1. **In contrast to the limiting case of the Giesekus model ($b \to \infty$), the Wiest model does not predict unphysical degree of shear-thinning in the steady shear viscosity for $a > 0.5$, Wiest (1989). Instead, it is found that the shear stress plateaus, corresponding to the steady shear viscosity decreasing as $\dot{\gamma}^{-1}$.**

The least square fitted value of b corresponds to very little extensibility which appears unphysical. Since we find no consistency in the magnitude of b, this parameter is allowed to float in the

following fits of the experimental data to the model.

The value of λ_H does seem to resemble the reptation time, and in the following fits the value of λ_H is held fixed on λ_a. The experimental data do, as mentioned before, show that the steady elongational viscosity scales with M for high Deborah numbers between PS390K and PS200K, and that the steady elongational viscosity $\bar{\eta} \sim \dot{\epsilon}^{-0.4}$. If it is assumed that the former also applies for $\bar{\eta}$ between the PS200K and PS100K, this can be used as a constraint fitting the steady viscosities for PS100K to the Wiest model. This is essentially the same as weighting the two largest elongational rates-measurements highest, since these do confirm the experimentally found molecular weight scaling between PS200K and PS100K, and also seem to decrease as $\bar{\eta} \sim \dot{\epsilon}^{-0.4}$. The fitted parameters of the Wiest model to the data, with the above mentioned constraint regarding molecular weight scaling, and the choices of λ_a are given in table 4 (see also figure **??**). The blend data for Blend 1, 2 and 3 are least square fitted to the Wiest model by using two time constants and two zero shear viscosities, but no constrains on the molecular weight scaling as seen in the figures **??**, **??** and **??**.

From table 4 for the monodisperse melts, it is seen that the value of a is unity for PS390K and gradually decreases as the molecular weight goes down, ending at $a = 0.14$ for PS50K, indicating that the degree of molecular anisotropy in the drag-force falls as molecular weight goes down, which was expected due to the higher density of dangling ends. The fitted values of b show no general tendency. We have also included the values of the maximum in the steady elongational viscosity relative to $3\eta_0$, and the maximum in $\bar{\eta}_{max}/(3\eta_0)$ is somehow inversely proportional to a. The strain hardening behaviour we see for the low molecular weight melts and the bidisperse blends is therefore in the terms of the Wiest model related to the amount of isotropy in the elongated melt.

The results for the blends show that it is possible to fit the data successfully to a two-mode Wiest model to the Blend 3-melt but not to the Blend 1-melt. If a single-mode fit is used instead, with all the parameters varying, a much better fit is obtained.

6 Conclusion

The steady elongational viscosity of two moderately entangled monodisperse polystyrene melts, with molecular weights of $52\,{}^{\mathrm{kg}}/_{\mathrm{mole}}$ and $103\,{}^{\mathrm{kg}}/_{\mathrm{mole}}$, have been found for elongational deformation rates ranging from $\dot{\epsilon} = 0.003s^{-1}$ to $\dot{\epsilon} = 0.3s^{-1}$. It is observed, that the steady elongational viscosity vs. elongational rate goes through a maximum, and followed by a decrease where the elongational rate scales as $\bar{\eta} \sim M_w\dot{\epsilon}^{0.4}$ for large elongational rates. The maximum is the result of fewer entanglements in these melts, in agreement with the predictions of Marrucci and Iannirubertо (2004).

The steady elongational viscosity has also been measured for bidisperse blends of a high and a low molecular weight monodisperse polystyrene. Here we also observe a maximum in the steady elongational viscosity vs. elongational rate. This maximum, relative to three times the zero shear viscosity, increase as the concentration of high molecular weight chains decrease. This observation is contrary to that found by Wagner et al. (2005), who found that the strain hardening increased with increasing concentration of ultra high molecular weight polystyrene. The molar masses in their studies are, however, well above $250\,{}^{\mathrm{Kg}}/_{\mathrm{mole}}$ which may be argued to be the upper limit for the application of the Weist model, see appendix (**??**). Conversely the maximum increases with reduced molecular weight of the low molecular weight chains.

The maximum found for bidisperse polymer blends indicates a qualitative difference between monodoisperse and bidisperse melts. This is different from the corresponding situation between monodisperse and bidisperse solutions (Ye et al. 2003).

The fact that the steady elongational viscosity of a blend of long (390kg/mole) and short polystyrene chains exhibits a maximum as function of elongation rate while the melt of pure long chains does not, may be interpreted in terms of the Wiest dumbbell model that combines the Giesekus anisotropic friction concept with finite extensibility. Indeed the pure melt of long chains has a large potential for anisotropic drag corresponding to the Giesekus parameter $a = 1$. Conversely in blends with a significantly lower molar mass or even solutions, the long chains will encounter an environment with less potential for anisotropy. Basically the long chains undergo stretching at rates at which the shorter chains are not oriented thereby providing an isotropic drag.

7 Acknowledgments

The authors gratefully acknowledge financial support to the Graduate School of Polymer Science from Danish Research Training Council and the Danish Technical Research Council to the Danish Polymer Centre.

8 Appendix

8.1 Behaviour of the Wiest-model for $\dot{\epsilon} \to \infty$

The constitutive equation for homogeneous steady flow of the Wiest model is:

$$Z\boldsymbol{\tau_p} + \lambda_H \boldsymbol{\tau_{(1)}} - \frac{aZ}{nkT}(\boldsymbol{\tau_p}\boldsymbol{\tau_p}) = -nkT\lambda_H\dot{\boldsymbol{\gamma}} \tag{17}$$

In strong uniaxial elongation, steady flows, the only stress contribution to the forces in the melt is τ_{zz}. To solve $\tau_{p,zz}$ the variable substitution $y = -\tau_{p,zz}/(nkT)$, and $x = \lambda_H\dot{\epsilon}$ is introduced. The stress in the zz-direction then becomes:

$$-\frac{ay^3}{b} + \frac{y^2}{b} + 2xy + 2x = 0 \tag{18}$$

Since τ_{zz} in stretching is negative, $y > 0$ for all values of x. It is assumed that for large elongational rates, the viscosity, and thereby also y behaves as a power law-function i.e.: $y \sim Ax^\alpha$ for $x \to \infty$. Substituting this into equation (**??**) we get:

$$-\frac{aA^3x^{3\alpha}}{b} + \frac{A^2x^{2\alpha}}{b} + 2Ax^{1+\alpha} + 2x = 0 \tag{19}$$

Since the absolute value of the stress, $|\tau_{zz}|$, and therefore y, increase for increasing elongational rates α must be larger than zero. The largest terms in equation (**??**) are $2Ax^{1+\alpha}$ and $-aA^3x^{3\alpha}/b$ which have to balance as $x \to \infty$, whereby we obtain $\alpha = 1/2$.

The pre-exponential terms also have to balance, for $x \to \infty$ so the parameter A becomes:

$$2A = \frac{a}{b}A^3 \Rightarrow A = \sqrt{\frac{2b}{a}} \tag{20}$$

The final asymptotic result is that:

$$\frac{\bar{\eta}}{nkT\lambda_H} = \sqrt{\frac{2b}{a}}\,(\lambda_H\dot{\epsilon})^{-1/2} \quad \text{for} \quad \dot{\epsilon} \to \infty \tag{21}$$

The modified Giesekus model thereby gives a physical explanation for the fact, that $\bar{\eta} \sim \dot{\epsilon}^{-1/2}$ for high elongational rates whereas the simple Giesekus model predicted $\bar{\eta}$ as having a finite limit for infinite $\dot{\epsilon}$.

8.2 Molecular interpretation of the finite extensibility b-parameter

We apply the Wiest model to a representative single entangled tube segment of the melt. The chain in the tube segment is modeled as a FENE spring with maximum length Q_0 and spring constant H_{seg} given by:

$$Q_0 = N_{k,seg} L_k \tag{22}$$

and

$$H_{seg} = \frac{3kT}{N_{k,seg} L_k^2} \tag{23}$$

where $N_{k,seg}$ is the number of Kuhn steps in entanglement segment, and L_k is the length of each Kuhn step. From these equations the constant b is defined, which yields a simpler expression:

$$b \equiv \frac{H_{seg} Q_0^2}{kT} = 3N_{k,seg} \tag{24}$$

The finite strain extensibility of an entanglement segment is given by $\exp(\epsilon_{max}) = \sqrt{N_{k,seg}}$**, Fang (2000), which means that the an in the affine limit, that is at infinite elongational rate, the segment has reached its maximum stretch at**

$$\epsilon_{max} = \frac{1}{2} \ln N_{k,seg} = \frac{1}{2} \ln \left(\frac{1}{3} b \right) \tag{25}$$

.

8.3 Scaling of steady state stress with M_w in the Wiest model

For an entangled polymer melt, the pre factor scale for stress is independent of molecular weight: $nkT \equiv G_N^0 = \rho RT/M_e$. With respect to the time constant λ_H, the relevant times to consider would be either the reptation, which is the characteristic time of the entire chain in the constrained tube taken from the Doi-Edwards interpretation of a polymer melt, or the Rouse time, which is a time constant for the stretching of the entangled segment between two segments. It makes sense in the Wiest model to choose the Rouse time as λ_H since it describes stretching which would make $\lambda_H \sim M_w^2$. But fitting showed that $\lambda_H \simeq \lambda_a$ which suggests that λ_H scales as the Doi-Edwards reptation time i.e. $\lambda_H \sim M_w^3$. **Of course, such apparent inconsistencies are inevitable with a dumbbell-based segment-level model. More detailed constitutive models for monodisperse melts (Marrucci and Iannirubertо 2004) recognize that the time-scales for orientation and chain-stretching scale differently with molecular weight. This is beyond the scope of the present discussion. We seek simply to show that a simple model with anisotrpic drag such as the Wiest model is capable of describing the experimental observations in pure melts and in blends. The steady stress scaling then become:**

$$\begin{aligned} (\sigma_{zz} - \sigma_{xx}) = \bar{\eta}\dot{\epsilon} = G_N^0 \quad &\cdot \quad \lambda_H^{1/2} \quad \cdot \quad b^{1/2} \quad \cdot \quad a^{-1/2}\dot{\epsilon}^{1/2}\sqrt{2} \\ \sim (M_w^0) \quad &\cdot \quad (M_w^3)^{1/2} \quad \cdot \quad (M_w^0)^{1/2} \quad \cdot \quad (M_w^x)^{-1/2} \end{aligned} \tag{26}$$

Assuming that the stress scales as $(\sigma_{zz} - \sigma_{xx}) \sim M_w \dot{\epsilon}^{1/2}$ an expression for molecular weight scaling-factor x of a is found using equation (**??**) to be $a \sim M_w^1$. This is only valid as long as $a \leq 1$.

Figure **??** below shows the fitted values of a as function of the molecular weight M_w. The solid line is the best linear fit against molecular weight, i.e. $a = AM_w^1$.

It is not possible to validate the molecular weight scaling of a from the plot, since only three data points are available. But the plot does indicate, that the Wiest model cannot be applied as constitutive equation of polystyrenes with molecular weights more than around 365 $^{\text{kg}}/_{\text{mole}}$ and hereby explaining why the fit for the steady elongational viscosity for PS390K was so poor. This indicates that the drag anisotropy saturates for polystyrenes with molecular weights above 365 $^{\text{kg}}/_{\text{mole}}$.

References

[1] Bach, A., Rasmussen, H. K., and Hassager, O., "Extensional viscosity for polymer melts measured in the filament stretching rheometer, " Journal of Rheology **47**, 429-441 (2003)

[2] Bach, A., Almdal, K., Rasmussen, H. K. and Hassager, O., "Elongational Viscosity of Narrow Molar Mass Distribution Polystyrene, " Macromolecules **36**, 5174-5179 (2003a).

[3] Baumgaertel, M., Schausberger, A., Winter, H. H., "The relaxation of polymers with linear flexible chains of uniform length, " Rheol. Acta **29**, 400-408 (1990).

[4] Bird, R. B., Curtiss, C. F., Armstrong, R. C. and Hassager, O., "Dynamics of Polymeric Liquids". John Wiley & Sons. Volume 2 Kinetic Theory (1987).

[5] des Cloizeaux, J., "Double reptation vs. simple reptation in polymer melts, ", Europhysics Letters **5**, 437-442 (1988).

[6] Doi, M. and Edwards, S. F., "The Theory of Polymer Dynamics", Clarendon Press: Oxford, 1986.

[7] Doi, M., "Introduction to Polymer Physics"; Clarendon Press: Oxford, 1992.

[8] Doi, M, Graessley, W.W., Helfand, E. and Pearson, D.S., "Dynamics of Polymers in Polydisperse Blends", Macromolecules **1987**, 20, 1900-1906.

[9] Eriksson, T. and Rasmussen, H. K., "The effects of polymer melt rheology on the replication of surface microstructures in isothermal moulding, " Journal of Non-Newtonian Fluid Mechanics **127**, 191-200 (2005).

[10] Fang, J., Kröger, M., Öttinger, H. C., "A thermodynamically admissible reptation model for fast flows of entangled polymers. II. Model predictions for shear and extensional flows, " Journal of Rheology **44**, 1293-1317 (2000).

[11] Ferry, J., "Viscoelastic Properties of Polymers"; Wiley: New York, 1980

[12] Fetters, L. J., Lohse, D. J., Richter, D., Witten, T. A. and Zirkel, A., "Connection between polymer molecular weight, density, chain dimensions, and melt viscoelastic properties," Macromolecules **27**, 4639 (1994).

[13] Giesekus, H., "A simple constitutive equation for polymer fluids based on the concept of deformation-dependent tensorial mobility, " Journal of Non-Newtonean Fluid Mechanics **11**, 69-109, (1982).

[14] Gupta, R. K., Nguyen, D. A. and Sridhar, T., "Extensional viscosity of dilute polystyrene solution - effect of concentration and molecular weight, " Phys. Fluids **12**, 1296-1318 (2000).

[15] Ianniruberto, G., Marrucci, G., "A simple constitutive equation for entangled polymers with chain stretch," Journal of Rheology **45**, 1305-1318 (2001).

[16] Jackson, J. K. and Winter, H. H., "Entanglement and Flow Behavior of Bidisperse Blends of Polystyrene and Polybutadiene," Macromolecules **28**, 3146-3155 (1995).

[17] Kolte, M. I., Rasmussen, H. K., and Hassager, O., "Transient filament stretching rheometer II: Numerical simulation," Rheol. Acta **36**, 285-302 (1997).

[18] Likhtman, A. "Single-Chain Slip-Link Model of Entangled Polymers: Simultaneous Description of Neutron Spin-Echo, Rheology, and Diffusion," Macromolecules **38**, 6128-6139 (2005).

[19] Lee, J.H., Fetters, L.J., Archer, L.A. and Halasa, A.F., "Tube dynamics in binary polymer blends", Macromolecules, **38**, 3917-3932, (2005).

[20] Luap C., C. Müller, T. Schweizer, D. C. Venerus, "Simultaneous stress and birefringence measurements during uniaxial elongation of polystyrene melts with narrow molecular weight distribution," Rheologica Acta **45**, 83-91 (2005).

[21] Marrucci, G., Grizzuti, N., "Fast flows of concentrated polymers- Predictions of the tube model on chain stretching ," Gazz. Chim. Ital. **118**, 179-185 (1988).

[22] Marrucci, G. and Ianniruberto, G., "Interchain Pressure Effect in Extensional Flows of Entangled Polymer Melts," Macromolecules, **37**, 3934-3942 (2004).

[23] Mead, D. W., Larson, R. G. and Doi, M., "A Molecular Theory for Fast Flows of Entangled Polymers, " Macromolecules **31**, 7895-7914 (1998)

[24] Milner, S. T., McLeish, T. C. B.,"Reptation and contour-length fluctuations in melts of linear polymers,". Physical Review Letters **81**, 725-728 (1998).

[25] Ndoni, S., Papadakis, C. M., Bates, F. S. and Almdal, K., "Laboratory-scale setup for anionic polymerization under inert atmosphere," Rev. Sci. Instrum. **66**, 1090-1095, (1995).

[26] Park, S.J, Larson, R.G., "Tube Dilation and Reptation in Binary Blends of Monodisperse Linear Polymers," Macromolecules (2004), **37**, 597.

[27] Rasmussen, H.K., and Hassager, O., "The role of surface tension on the elastic decohesion of polymeric filaments, " Journal of Rheology **45**, 527-537 (2001)

[28] Rasmussen, H. K., Nielsen, J. K., Bach, A. and Hassager, O., "Viscosity overshoot in the start-up of uni-axial elongation of LDPE melts," Journal of Rheology **49**, 369-381 (2005).

[29] Rasmussen, H. K. and Hassager, O., "The role of surface tension on the elastic decohesion of polymeric filaments ," Journal of Rheology **45**, 527 (2001).

[30] Rasmussen, H. K., Christensen, J. H., Gottsche, S. J. "Inflation of polymer melts into elliptic and circular cylinders, " Non-Newtonian Fluid Mech. **93**, 245-263 (2000).

[31] Schausberger, A. and Schindlauer, G., "Linear elastico-viscous properties of molten standard polystyrenes, " Journal of Rheology **24**, 220-227 (1985)

[32] Schieber, J., Neergaard, J., Gupta, S., "A full-chain, temporary network model with sliplinks, chain-length fluctuations, chain connectivity and chain stretching," Journal of Rheology **47**, 213-233 (2003).

[33] Spiegelberg, S.H., and McKinley, G. H., "The role of end-effects on measurements of extensional viscosity in filament stretching rheometers," Journal of Non-Newtonian Fluid Mechanics **64**, 229-267 (1996).

[34] Struglinski, M. J., and Graessley, W. W., "Effects of polydispersity on the linear viscoelastic properties of entangled polymers. 1. Experimental observations for binary mixtures of linear polybutadiene, " Macromolecules **18**, 2630-2643 (1988)

[35] Szabo, P., "Transient filament stretching rheometer part I: Force Balance analysis, " Rheologica Acta **36**, 277-284 (1997).

[36] Szabo P. and McKinley, G., "Filament stretching rheometer: inertia compensation revisited, " Rheologica Acta **42**, 269-272 (2003). (1985).

[37] Tanner, R. T. and Walters, K., "Rheology: An historical perspective, " Elserier, Amstadam (1998).

[38] Wagner, M. H., S. Kheirandish, K. Koyama, A. Nishioka, A. Minegishi and T. Takahashi, "Tensile stress overshoot in uniaxial extension of a LDPE melt, " Rheologica Acta **44** 235-243 (2005).

[39] Wagner, M. H., S. Kheirandish, O. Hassager, "Quantitative prediction of the transient and steady-state elongatiuonal viscosity of nearly monodisperse polystyrene melts" Journal of Rheology **49**, 1317-1327 (2005).

[40] Wagner, M. H., Raible, T. and Meissner, J., "Tensile stress overshoot in uniaxial extension of a LDPE melt, " Rheologica Acta **18** 427-428 (1979).

[41] Wagner, M. H., Rubio, P. and Bastian, H., "The molecular stress function model for polydisperse polymer melts with dissipative convective constraint release, " Journal of Rheology **45**, 1387-1412 (2001).

[42] Wiest, J. M., "A differential constitutive equation for polymer melts, " Rheologica Acta **28**, 4-12 (1989).

[43] Ye, X., Larson, R.G., Pattamaprom, C. and Sridhar, T., "Extensional properties of monodisperse and bidisperse polystyrene solutions, " Journal of Rheology **47**, 443-468 (2003).

9 Table

	Blend 1	Blend 2	Blend 3	Ye et al
w/w% PS50K	95.98	85.63	0	-
w/w% PS100K	0	0	85.98	-
w/w% PS390K	4.02	14.37	14.02	-
c_{PS390K}/c*	2.5	10	10	-
$M_w[kg/mol]$	65.3	100.3	143.1	-
G_r	0.499	0.499	0.064	0.0192

Table 1: Composition of Blend 1, Blend 2, Blend 3 and Ye et al.'s blend

Name	PS50K	PS100K	PS200K	PS390K	Blend 1	Blend 2	Blend 3
$M_w[kg/mol]$	51.7	102.8	200.0	390.0	65.3	100.3	143.1
M_w/M_n	1.026	1.022	1.040	1.060	1.218	1.683	1.248

Table 2: Molecular weights (M_w) and polydispersities (M_w/M_n) of the pure and blended polystyrene melts

Name	PS50K	PS100K	PS200K	PS390K	Blend 1	Blend 2	Blend 3
$\eta_{0,1}[MPas]$	0.82	7.88	82.9	724	0.78	1.02	5.97
$\eta_{0,2}[MPas]$	-	-	-	-	0.59	4.64	8.58
$\eta_0[MPas]$	0.82	7.88	82.9	724	1.37	5.66	14.6
$\lambda_{max,1}[s]$	12.8	158	1749	15441	12.2	17.4	122.1
$\lambda_{max,2}[s]$					2186	3182	5572
$\lambda_{a,1}[s]$	7.05	87.02	965	8517	6.73	9.60	67.4
$\lambda_{a,2}[s]$	-	-	-	-	1206	1755	3074
$G^0_{N1}[kPa]$	250	250	250	250	249	242	242
$G^0_{N2}[kPa]$	-	-	-	-	1.43	7.73	8.18
$G^0_N[kPa]$	250	250	250	250	250	250	250

Table 3: Linear viscoelastic properties of the pure and blended melts at 130°C. The constants in the BSW model are: $n_e = 0.23$, $n_g = 0.67$ and $\lambda_c = 0.4s$ as obtained from Jackson and Winter (1995) plus $G^0_N = 250kPa$

Name	PS50K	PS100K	PS200K	PS390K	Blend 1	Blend 2	Blend 3
w/w% PS50K					95.98	85.63	0
w/w% PS100K					0	0	85.98
w/w% PS390K					4.02	14.37	14.02
a	0.1372	0.2182	0.7033	1.000	$1.89 \cdot 10^{-4}$	$5.65 \cdot 10^{-4}$	0.1982
b	9.9	4.6	5.3	6.93	13.3	5.9	98.5
$\bar{\eta}_{max}/(3\eta_0)$	2.56	1.54	1.17	1	7.40	5.06	1.95

Table 4: The least square fitt of the Wiest model parameters a and b for the different melts together with dimensionless maximum in the steady elongational viscosity $\bar{\eta}_{max}/(3\eta_0)$

10 Figure captions

Figure 1: Results of linear viscoelastic measurements of G' as a function of the angular frequency ω. The measurements on the polystyrene melts were performed at 130, 150, and 170°C. The data are all time-temperature shifted to a reference temperature of $T_0 = 130$ °C.

Figure 2:Results of linear viscoelastic measurements of G'' as a function of the angular frequency ω. The measurements on the polystyrene melts were performed at 130, 150, and 170 °C. The data are all time-temperature shifted to a reference temperature of $T_0 = 130$ °C.

Figure 3: Corrected (equation **??**) transient extensional viscosity of PS50K and PS100K measured at different strain rates. Measurements were performed at 130 °C.

Figure 4: Same data as in figure **??** for PS50K but plotted as uncorrected transient extensional stress (equation **??**) against Hencky strain ϵ.

Figure 5: Same data as in figure **??** for PS100K but plotted as uncorrected transient extensional stress (equation **??**) against Hencky strain ϵ.

Figure 6: The steady stress divided with the plateau modulus against the Marrucci-Deborah number $\epsilon\tau_p$ for PS50K, PS100K, PS200K and PS390K.

Figure 7: Corrected transient extensional viscosity (equation **??**) of Blend 1 measured at different strain rates. Measurements were performed at 130 °C.

Figure 8: Same data as in figure **??** for Blend 1 but plotted as uncorrected transient extensional stress (equation **??**) against Hencky strain ϵ.

Figure 9: Corrected transient extensional viscosity (equation **??**) of Blend 3 measured at different strain rates. Measurements were performed at 130 °C.

Figure 10: Same data as in figure **??** for Blend 3 but plotted as the uncorrected transient extensional stress (equation **??**) against Hencky strain ϵ

Figure 11: Corrected (equation ??) transient extensional viscositis of Blend 1, Blend 2, PS50K and PS390K at $\dot{\epsilon} = 0.1s^{-1}$. The broken line is the Upper Convected Maxwell (UCM) prediction for $De = \lambda_{a,2,blend1} \cdot 0.1s^{-1} = 121$, the solid line is the UCM prediction for $De = \lambda_{a,2,blend2} \cdot 0.1s^{-1} = 176$, the dashed dot line is the UCM prediction for $De = \lambda_{a,1,PS390K} \cdot 0.1s^{-1} = 1544$. The dotted line is the neo-Hookean model with G = 250 kPa, cut off at ϵ_{max}. The values of three times the zero shear viscosity for each melt is showed on the right with punctured lines.

Figure 12: Steady extensional viscosity measurements of PS100K ($\circ$) measured at 130 °C. The solid line is the Wiest fit where a=0.1805, b=4.44 and $\lambda_H = 66.85s$. The dotted line is the Wiest fit where a=0.4055, b=66 and $\lambda_H = 105.7725s$.

Figure 13: Steady elongational viscosity as a function of the elongational rate for PS50K, PS100K, PS200K and PS390K. All measurements performed at 130°C. The solid lines are the predictions of the Wiest model.

Figure 14: Steady elongational viscosity against the elongational rate for Blend 3. All measurements performed at 130°C. The solid line is the overall prediction of the Wiest model, and the dashed lines are the individual contributions from the two individual polymer species.

Figure 15: Steady elongational viscosity against the elongational rate for Blend 2. All measurements performed at 130°C. The solid line is the overall prediction of the Wiest model, and the dashed lines are the individual contributions from the two individual polymer species.

Figure 16: Steady elongational viscosity against the elongational rate for Blend 1. All measurements performed at 130°C. The solid line is the overall prediction of the Wiest model, and the dashed lines are the individual contributions from the two polymers.

Figure 17: Least square fitted parameter of a against M_w. Solid line is a linear fit, $a = A(M_w)^1$.

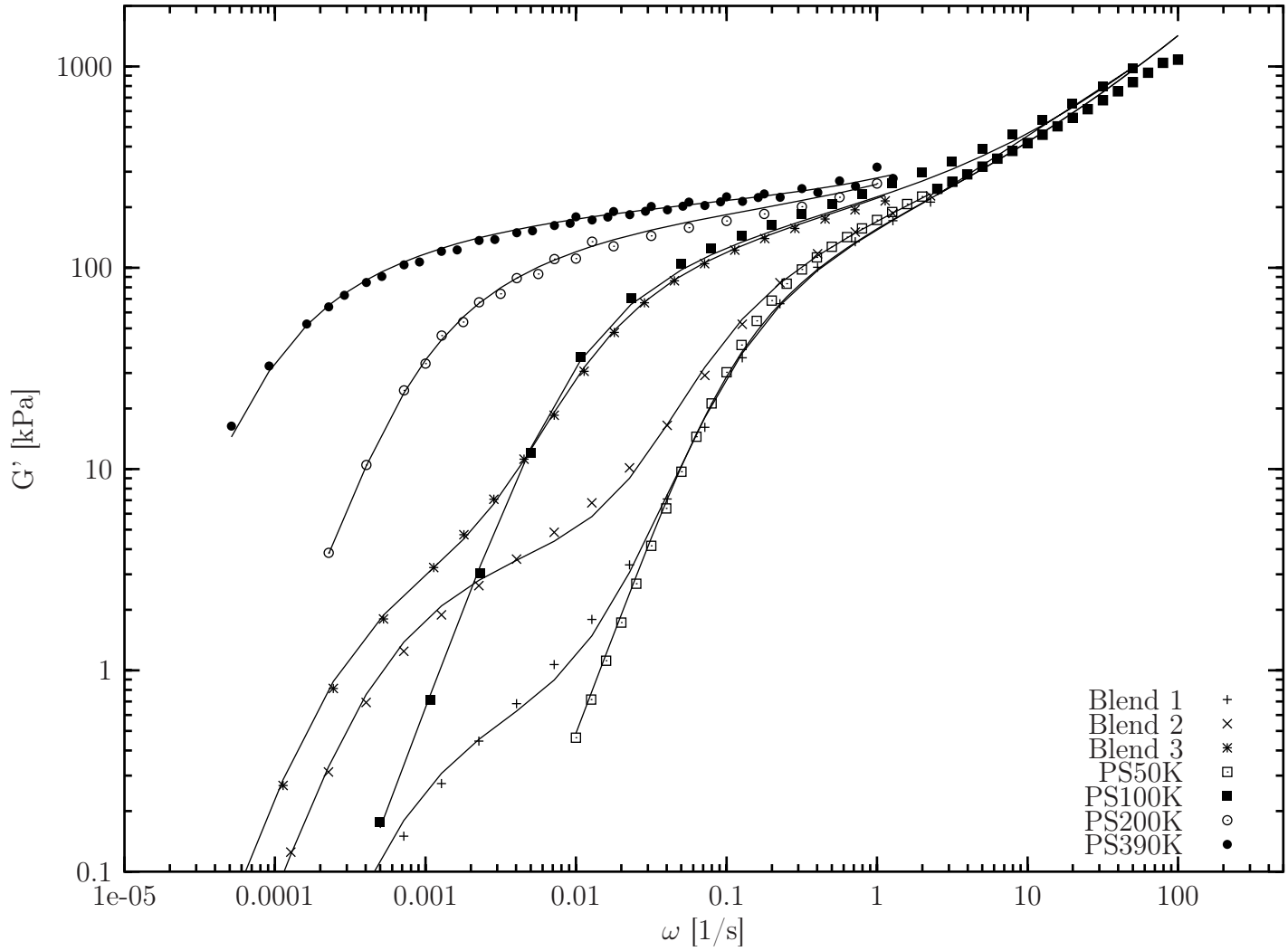
1000
100
10
1
0.1
G' [kPa]
1e-05
0.0001
0.001
0.01
0.1
1
10
100
ω [1/s]
Blend 1
Blend 2
Blend 3
PS50K
PS100K
PS200K
PS390K

Figure 1:

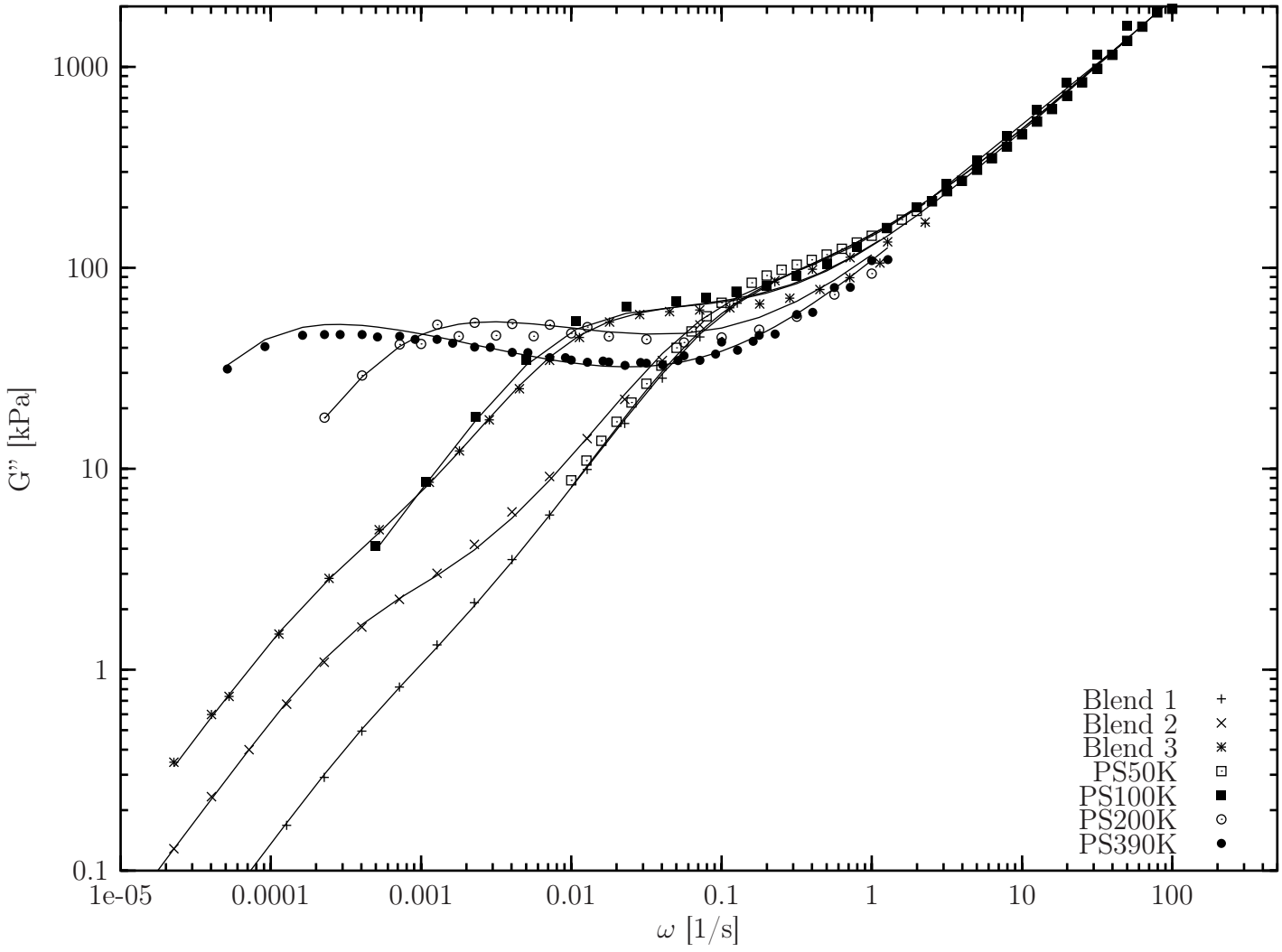
1000
100
10
1
0.1
G" [kPa]
1e-05
0.0001
0.001
0.01
0.1
1
10
100
ω [1/s]
Blend 1
Blend 2
Blend 3
PS50K
PS100K
PS200K
PS390K

Figure 2:

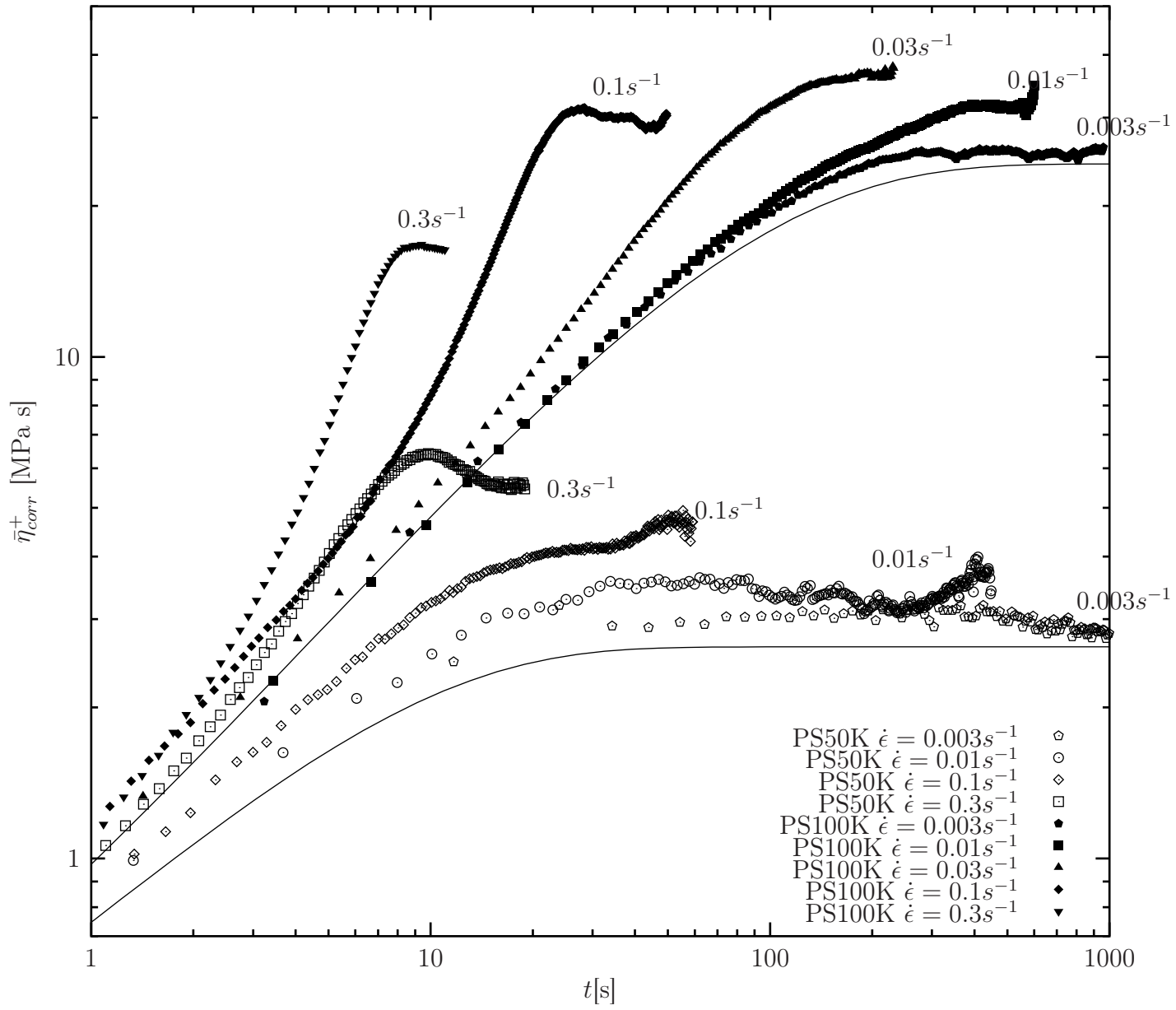
$0.03s^{-1}$
$0.1s^{-1}$
$0.01s^{-1}$
$0.003s^{-1}$
$0.3s^{-1}$
$0.3s^{-1}$
$0.1s^{-1}$
$0.01s^{-1}$
$0.003s^{-1}$
PS50K $\dot{\epsilon} = 0.003s^{-1}$
PS50K $\dot{\epsilon} = 0.01s^{-1}$
PS50K $\dot{\epsilon} = 0.1s^{-1}$
PS50K $\dot{\epsilon} = 0.3s^{-1}$
PS100K $\dot{\epsilon} = 0.003s^{-1}$
PS100K $\dot{\epsilon} = 0.01s^{-1}$
PS100K $\dot{\epsilon} = 0.03s^{-1}$
PS100K $\dot{\epsilon} = 0.1s^{-1}$
PS100K $\dot{\epsilon} = 0.3s^{-1}$
$\bar{\eta}^+_{corr}$ [MPa s]
10
1
1
10
100
1000
t[s]

Figure 3:

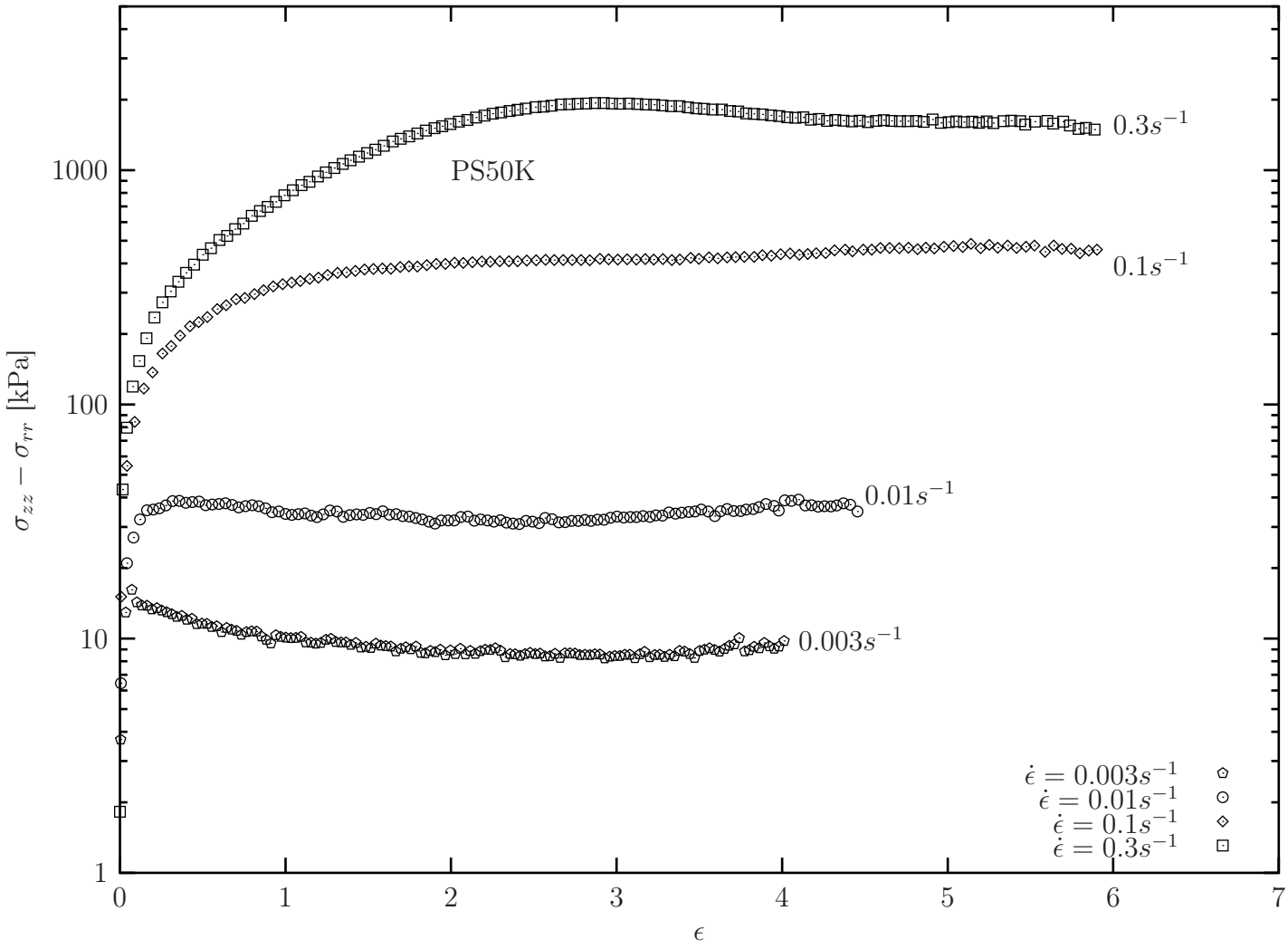
PS50K
$0.3s^{-1}$
$0.1s^{-1}$
$0.01s^{-1}$
$0.003s^{-1}$
$\dot{\epsilon} = 0.003s^{-1}$
$\dot{\epsilon} = 0.01s^{-1}$
$\dot{\epsilon} = 0.1s^{-1}$
$\dot{\epsilon} = 0.3s^{-1}$
$\sigma_{zz} - \sigma_{rr}$ [kPa]
ϵ
1000
100
10
1
0
1
2
3
4
5
6
7

Figure 4:

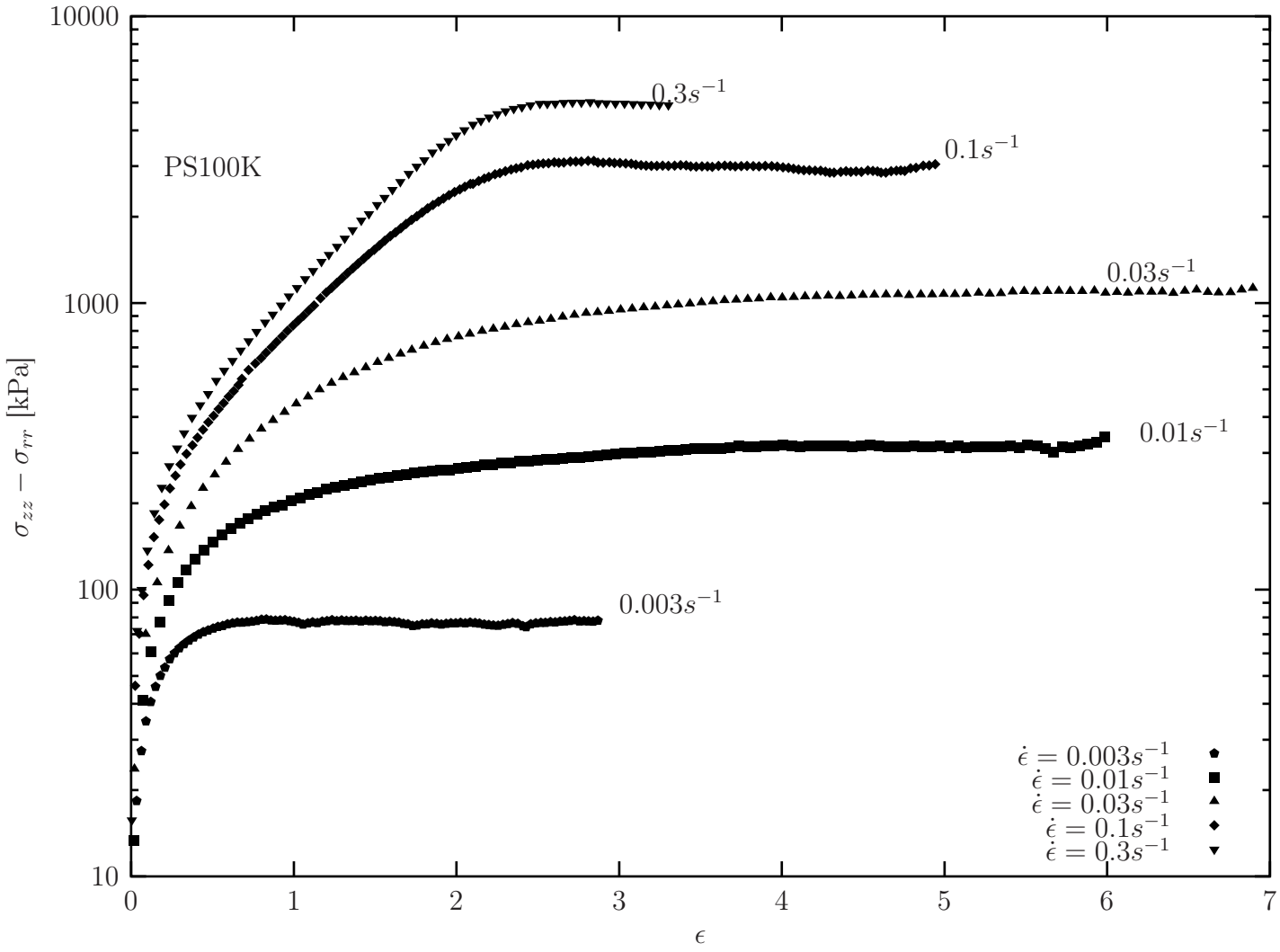
10000
1000
100
10
0
1
2
3
4
5
6
7
$\sigma_{zz} - \sigma_{rr}$ [kPa]
ϵ
PS100K
$0.3s^{-1}$
$0.1s^{-1}$
$0.03s^{-1}$
$0.01s^{-1}$
$0.003s^{-1}$
$\dot{\epsilon} = 0.003s^{-1}$
$\dot{\epsilon} = 0.01s^{-1}$
$\dot{\epsilon} = 0.03s^{-1}$
$\dot{\epsilon} = 0.1s^{-1}$
$\dot{\epsilon} = 0.3s^{-1}$

Figure 5:

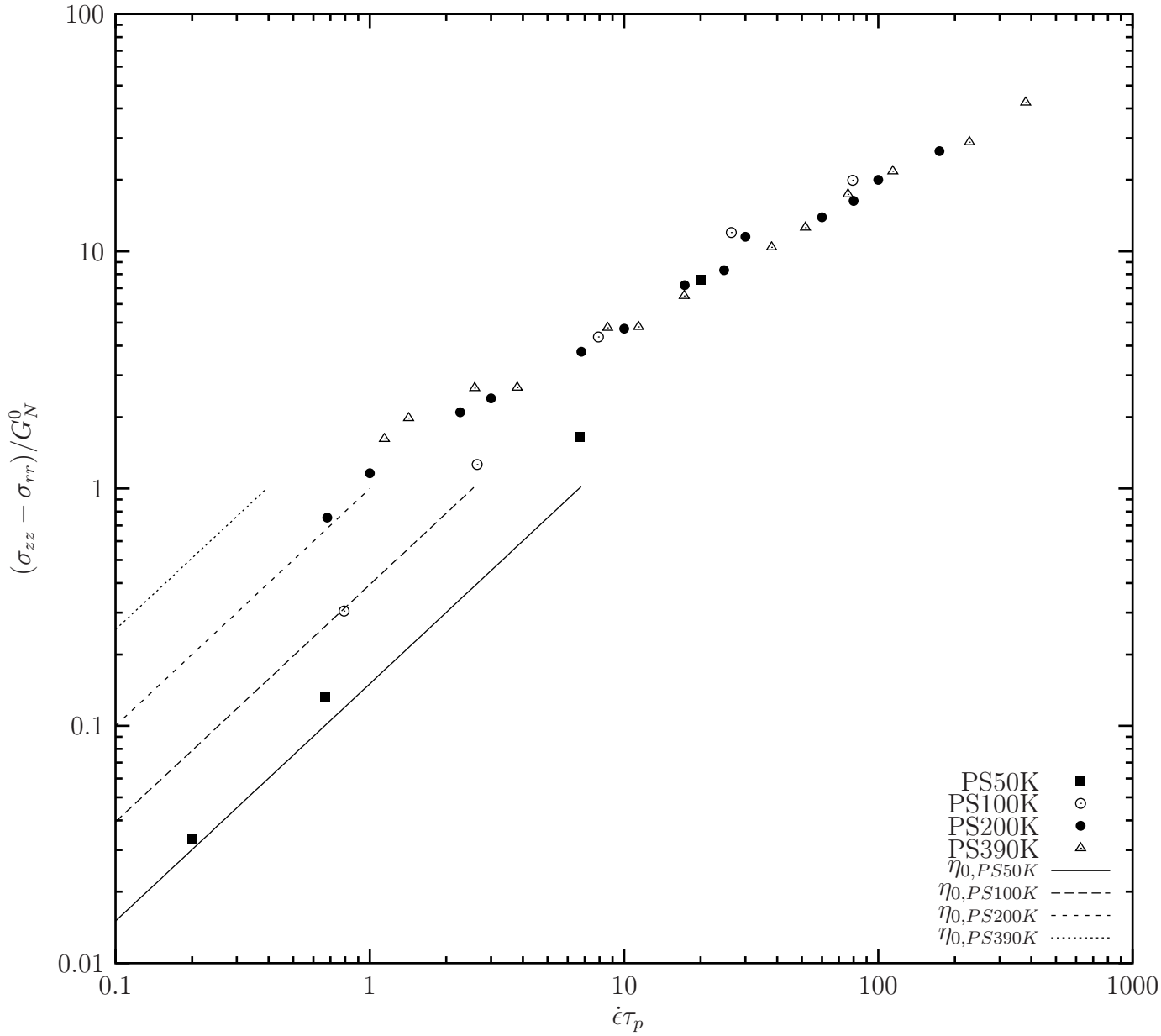
100
10
1
0.1
0.01
0.1
1
10
100
1000
$(\sigma_{zz} - \sigma_{rr})/G_N^0$
$\dot{\epsilon}\tau_p$
PS50K
PS100K
PS200K
PS390K
$\eta_{0,PS50K}$
$\eta_{0,PS100K}$
$\eta_{0,PS200K}$
$\eta_{0,PS390K}$

Figure 6:

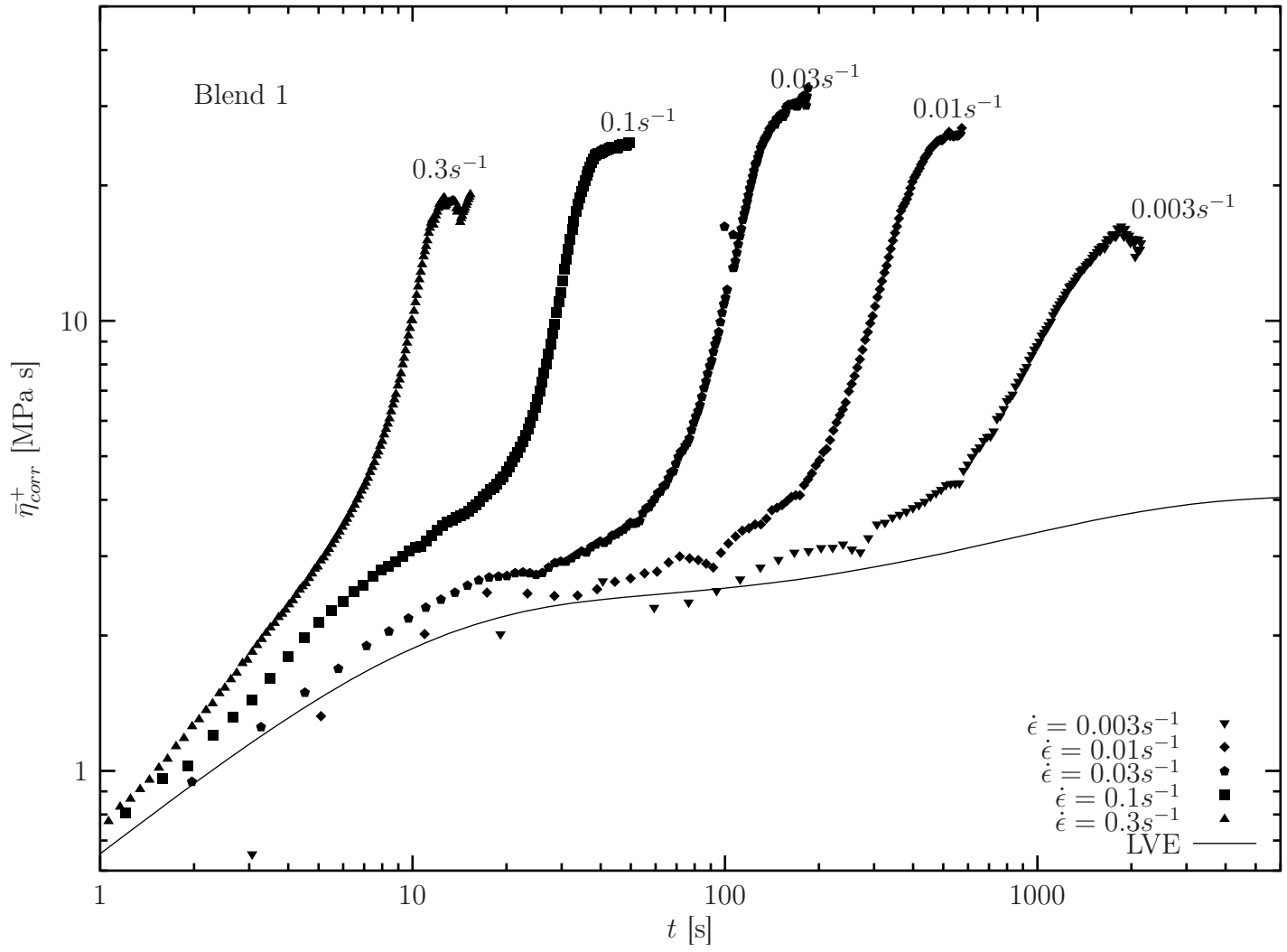
Blend 1
$0.3s^{-1}$
$0.1s^{-1}$
$0.03s^{-1}$
$0.01s^{-1}$
$0.003s^{-1}$
$\dot{\epsilon} = 0.003s^{-1}$
$\dot{\epsilon} = 0.01s^{-1}$
$\dot{\epsilon} = 0.03s^{-1}$
$\dot{\epsilon} = 0.1s^{-1}$
$\dot{\epsilon} = 0.3s^{-1}$
LVE
$\bar{\eta}^+_{corr}$ [MPa s]
t [s]
1
10
100
1000
1
10

Figure 7:

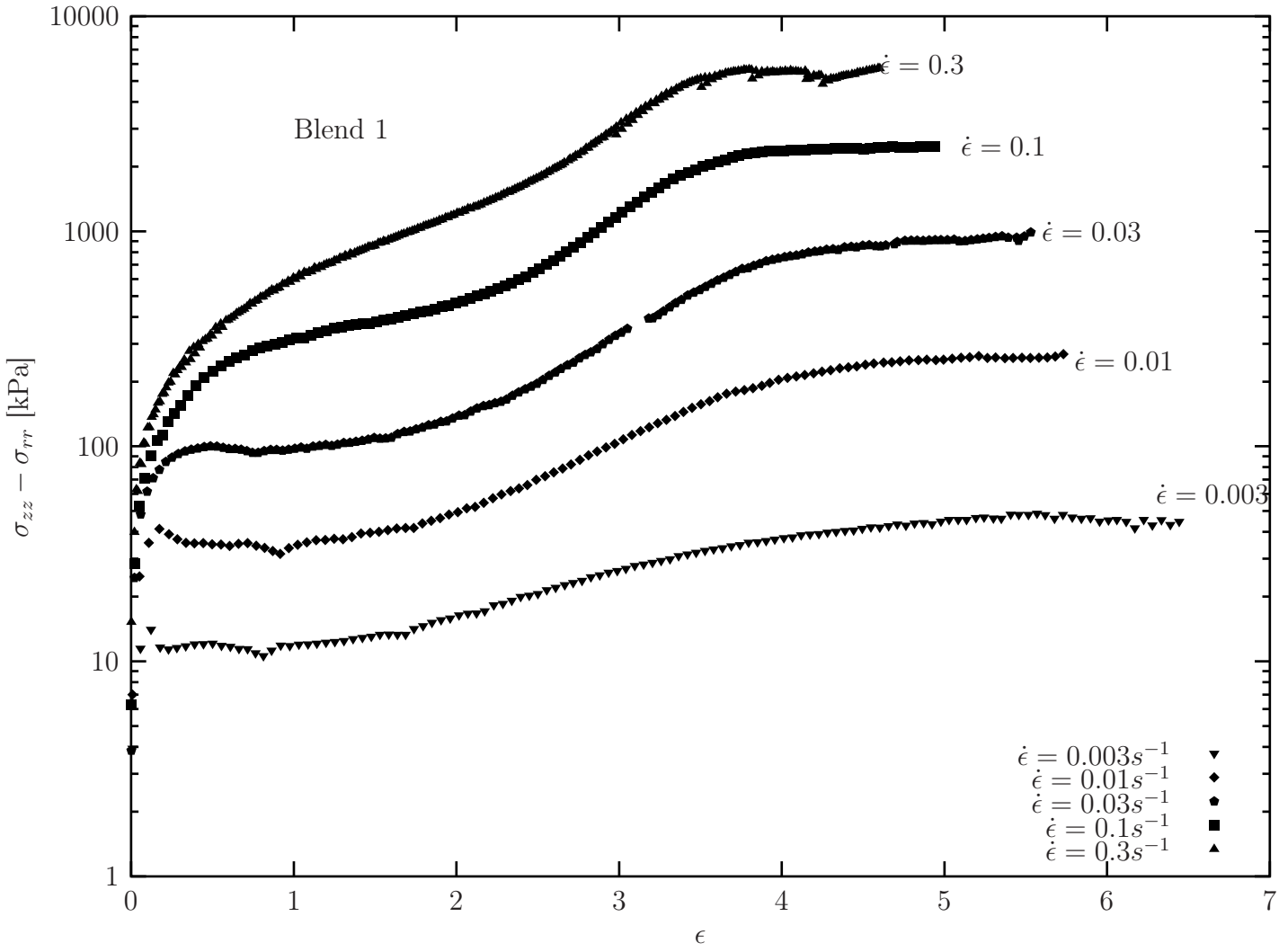
10000
1000
100
10
1
0
1
2
3
4
5
6
7
$\sigma_{zz} - \sigma_{rr}$ [kPa]
ϵ
Blend 1
$\dot{\epsilon} = 0.3$
$\dot{\epsilon} = 0.1$
$\dot{\epsilon} = 0.03$
$\dot{\epsilon} = 0.01$
$\dot{\epsilon} = 0.003$
$\dot{\epsilon} = 0.003s^{-1}$
$\dot{\epsilon} = 0.01s^{-1}$
$\dot{\epsilon} = 0.03s^{-1}$
$\dot{\epsilon} = 0.1s^{-1}$
$\dot{\epsilon} = 0.3s^{-1}$

Figure 8:

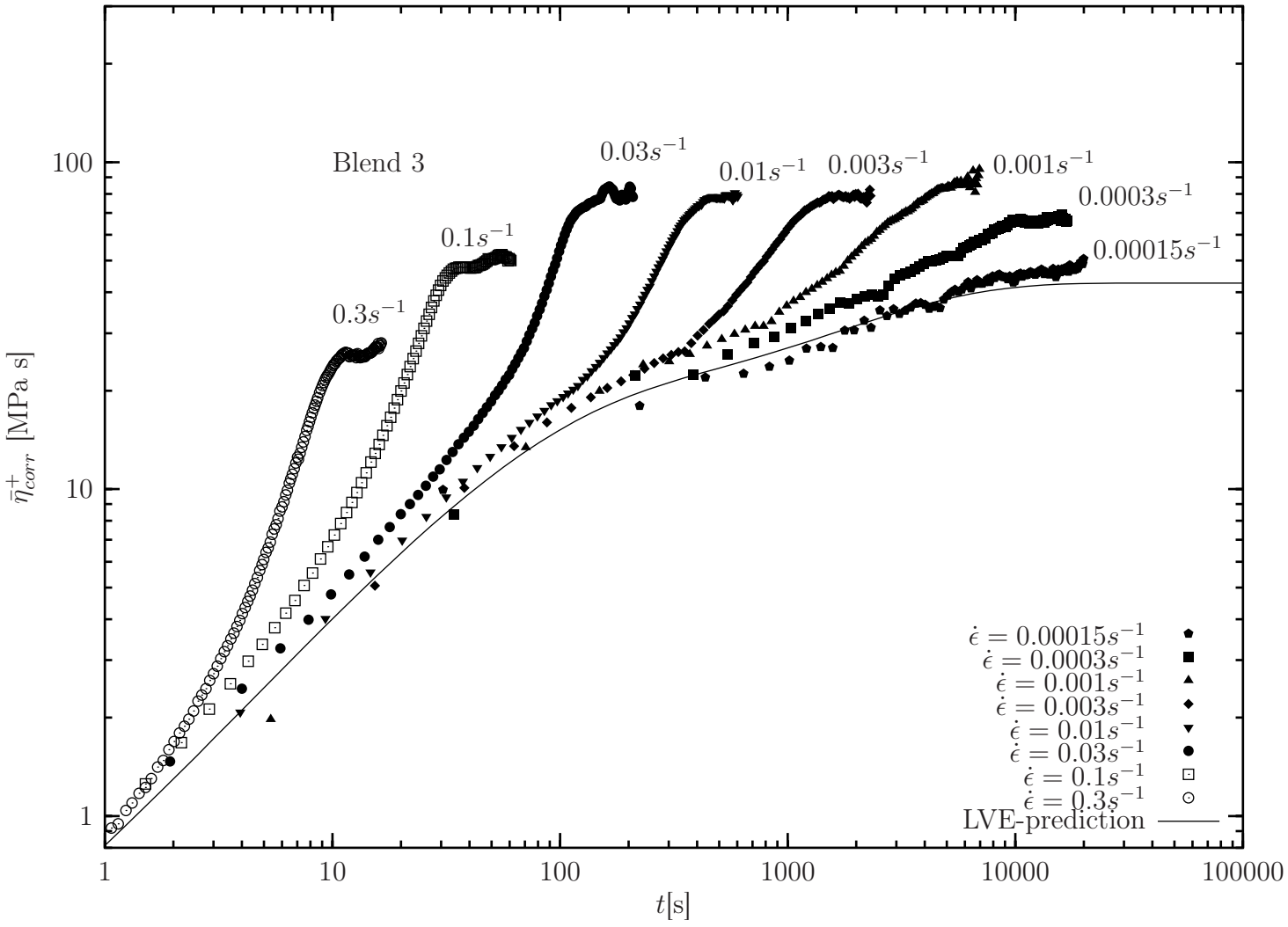
Blend 3
$0.03s^{-1}$
$0.01s^{-1}$
$0.003s^{-1}$
$0.001s^{-1}$
$0.0003s^{-1}$
$0.00015s^{-1}$
$0.1s^{-1}$
$0.3s^{-1}$
$\dot{\epsilon} = 0.00015s^{-1}$
$\dot{\epsilon} = 0.0003s^{-1}$
$\dot{\epsilon} = 0.001s^{-1}$
$\dot{\epsilon} = 0.003s^{-1}$
$\dot{\epsilon} = 0.01s^{-1}$
$\dot{\epsilon} = 0.03s^{-1}$
$\dot{\epsilon} = 0.1s^{-1}$
$\dot{\epsilon} = 0.3s^{-1}$
LVE-prediction
$\bar{\eta}^+_{corr}$ [MPa s]
t[s]
100
10
1
1
10
100
1000
10000
100000

Figure 9:

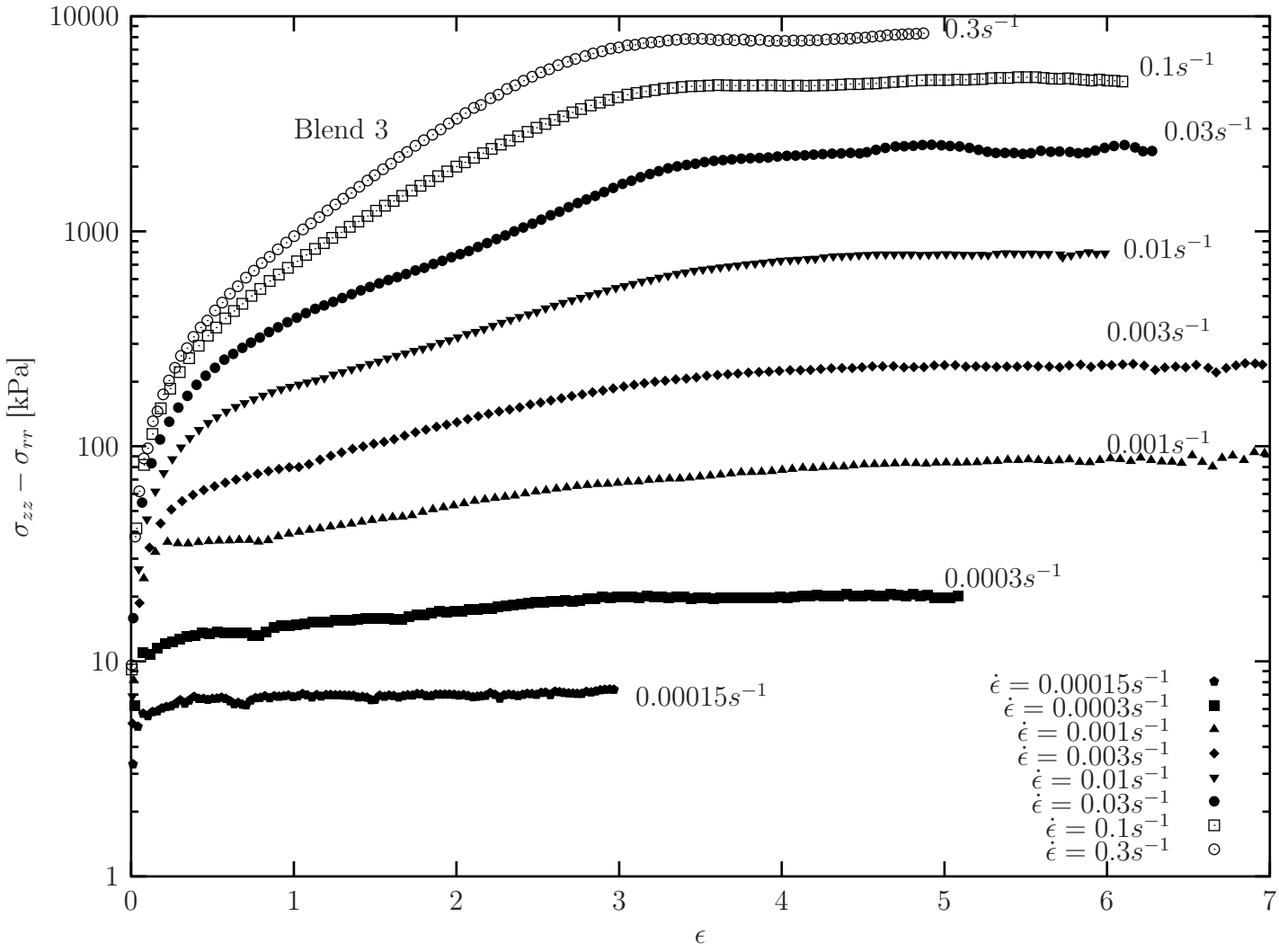
10000
1000
100
10
1
0
1
2
3
4
5
6
7
$\sigma_{zz} - \sigma_{rr}$ [kPa]
ϵ
Blend 3
$0.3s^{-1}$
$0.1s^{-1}$
$0.03s^{-1}$
$0.01s^{-1}$
$0.003s^{-1}$
$0.001s^{-1}$
$0.0003s^{-1}$
$0.00015s^{-1}$
$\dot{\epsilon} = 0.00015s^{-1}$
$\dot{\epsilon} = 0.0003s^{-1}$
$\dot{\epsilon} = 0.001s^{-1}$
$\dot{\epsilon} = 0.003s^{-1}$
$\dot{\epsilon} = 0.01s^{-1}$
$\dot{\epsilon} = 0.03s^{-1}$
$\dot{\epsilon} = 0.1s^{-1}$
$\dot{\epsilon} = 0.3s^{-1}$

Figure 10:

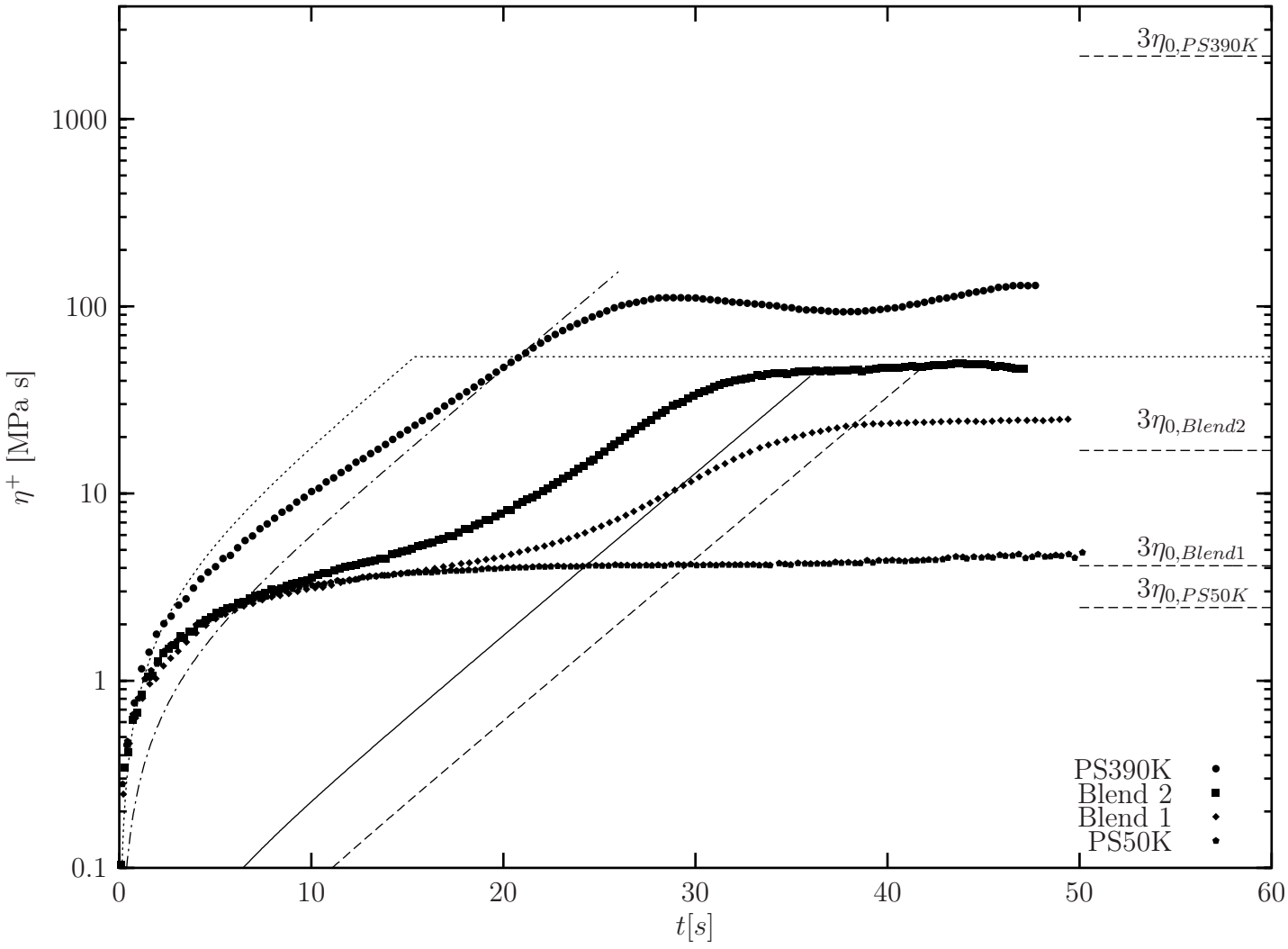
$3\eta_{0,PS390K}$
$3\eta_{0,Blend2}$
$3\eta_{0,Blend1}$
$3\eta_{0,PS50K}$
PS390K
Blend 2
Blend 1
PS50K
η^+ [MPa s]
$t[s]$
1000
100
10
1
0.1
0
10
20
30
40
50
60

Figure 11:

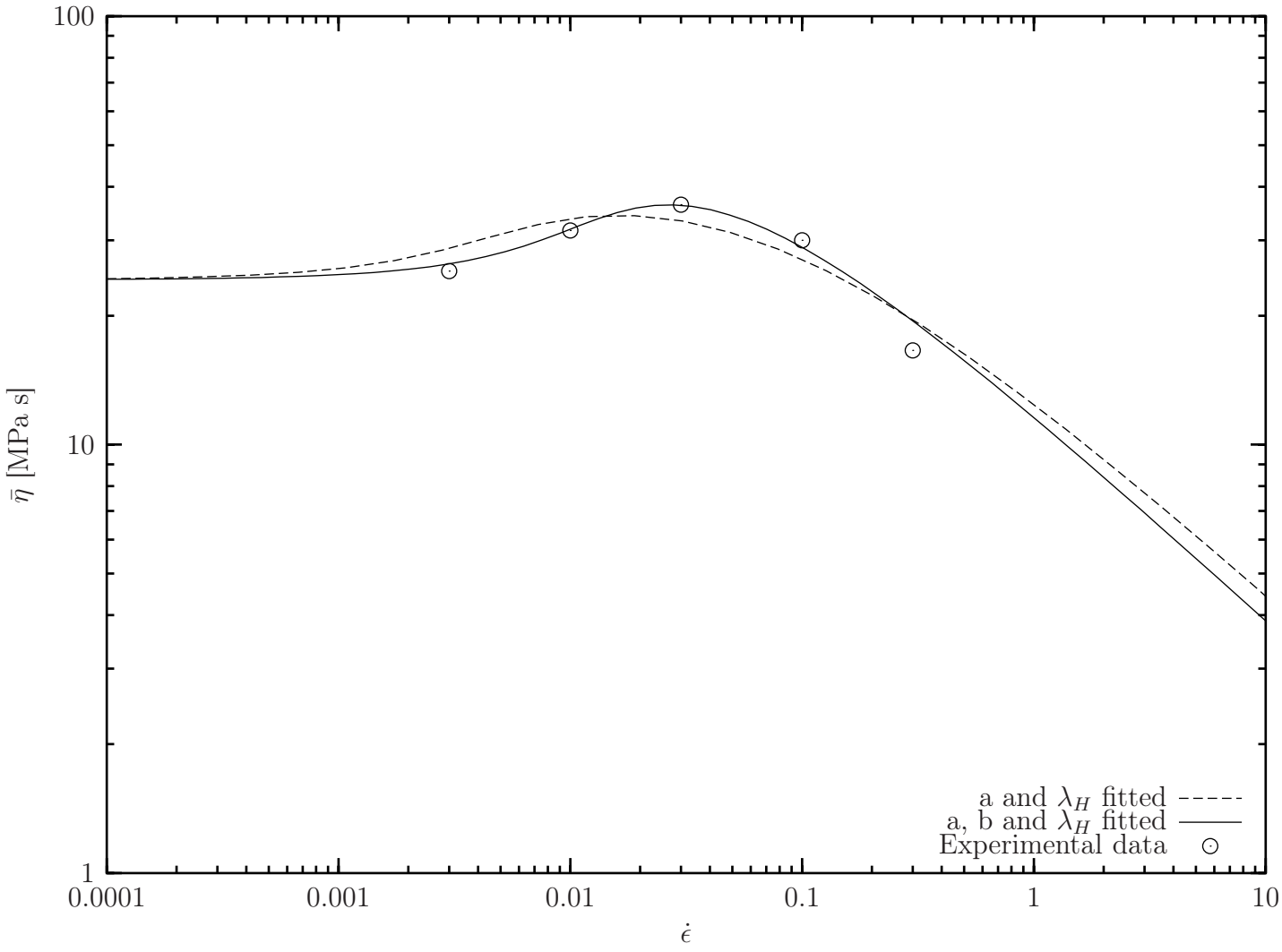
100
10
1
0.0001
0.001
0.01
0.1
1
10
$\bar{\eta}$ [MPa s]
$\dot{\epsilon}$
a and λ_H fitted
a, b and λ_H fitted
Experimental data

Figure 12:

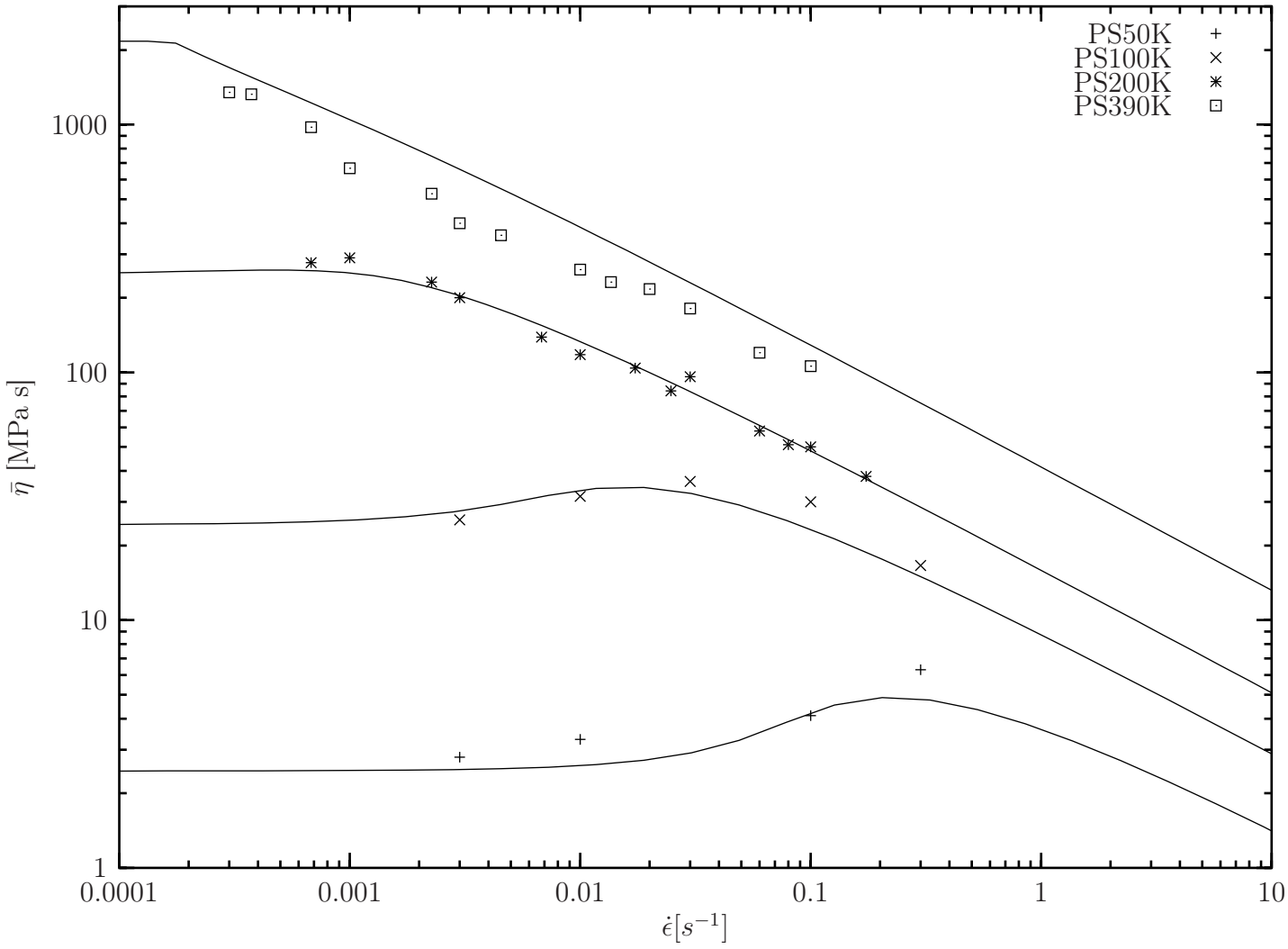
PS50K
PS100K
PS200K
PS390K
1000
100
10
1
$\bar{\eta}$ [MPa s]
0.0001
0.001
0.01
0.1
1
10
$\dot{\epsilon}[s^{-1}]$

Figure 13:

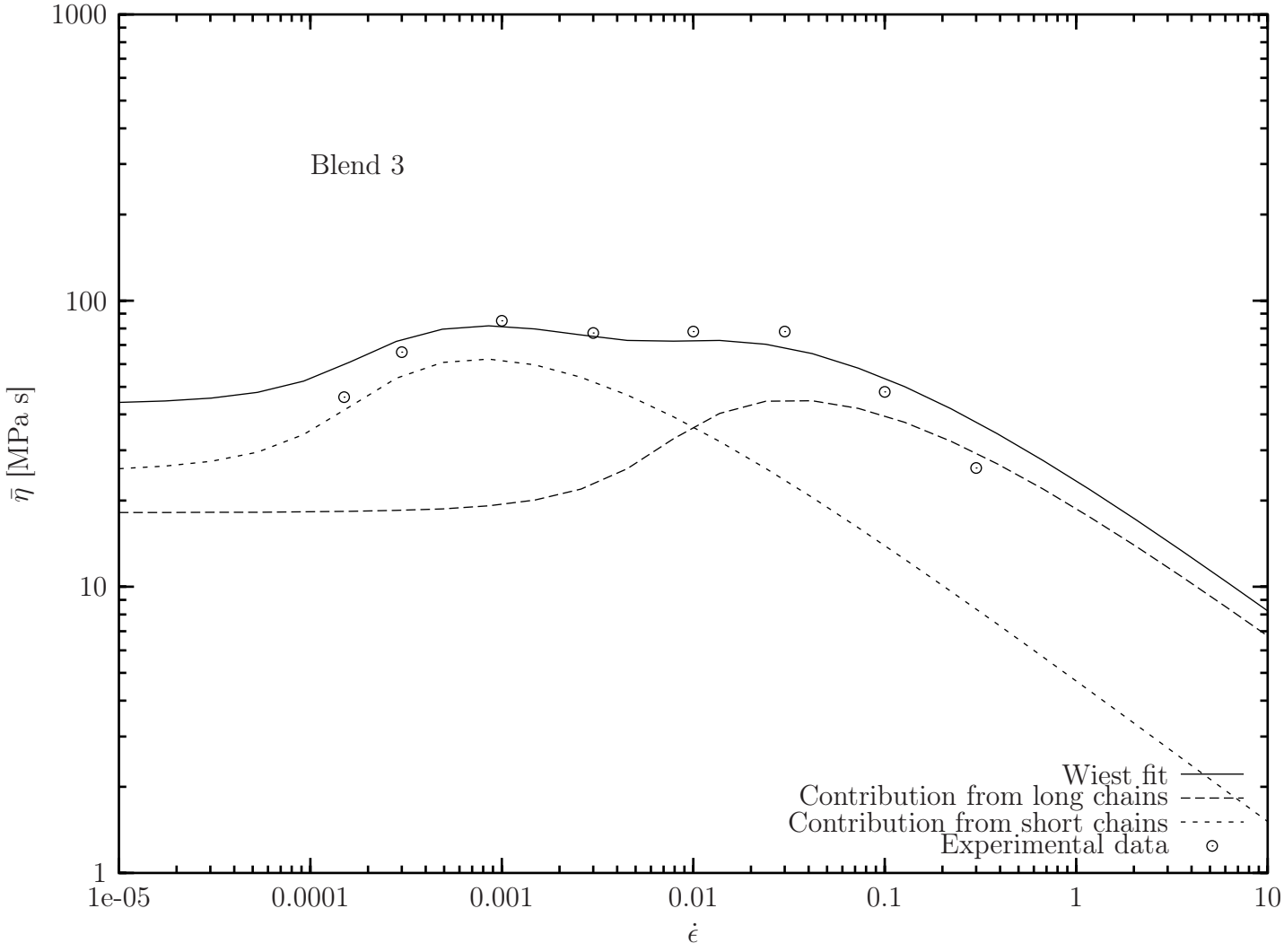
1000
100
10
1
1e-05
0.0001
0.001
0.01
0.1
1
10
Blend 3
$\bar{\eta}$ [MPa s]
$\dot{\epsilon}$
Wiest fit
Contribution from long chains
Contribution from short chains
Experimental data

Figure 14:

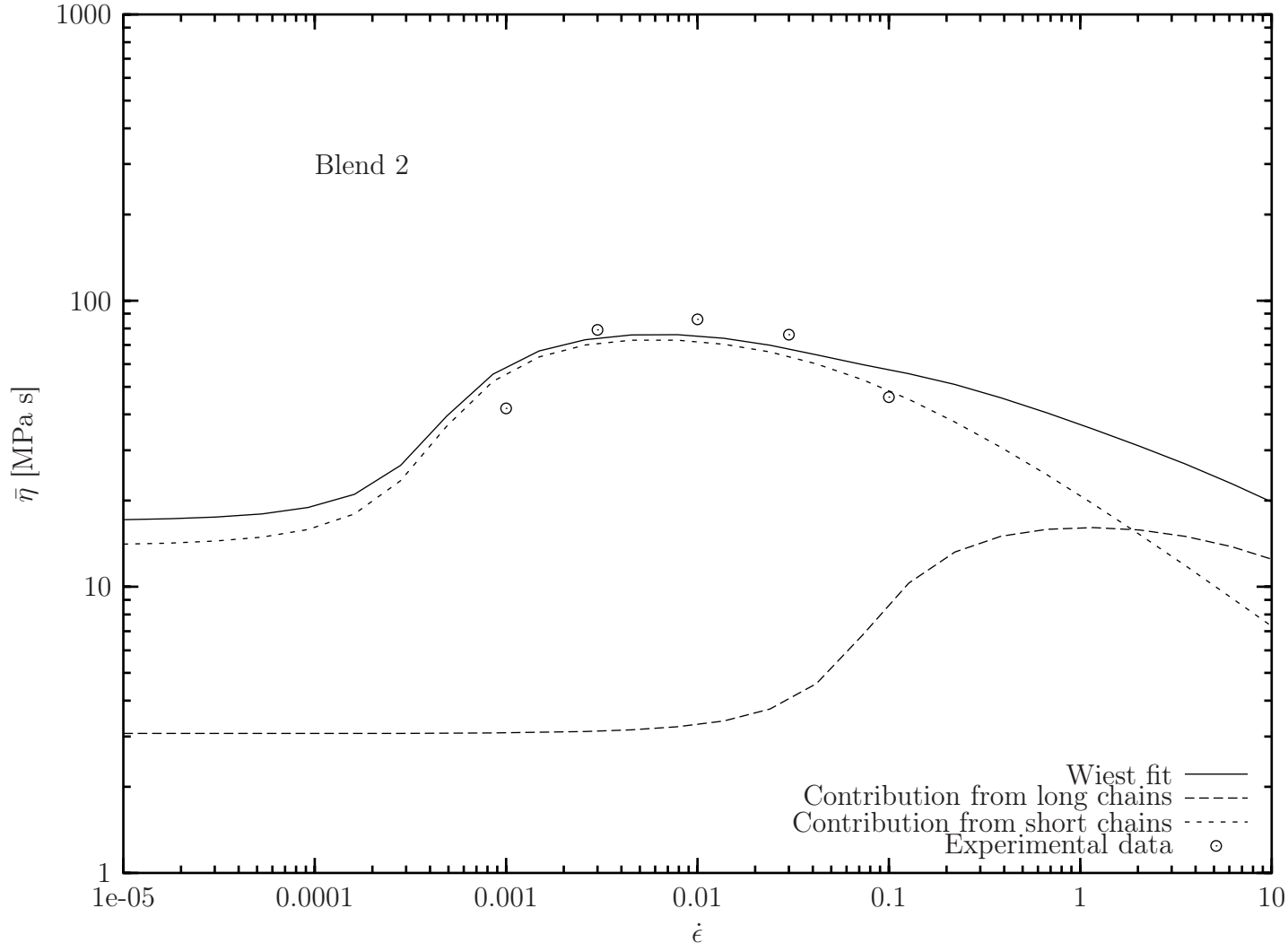
Blend 2
1000
100
10
1
1e-05
0.0001
0.001
0.01
0.1
1
10
$\bar{\eta}$ [MPa s]
$\dot{\epsilon}$
Wiest fit
Contribution from long chains
Contribution from short chains
Experimental data

Figure 15:

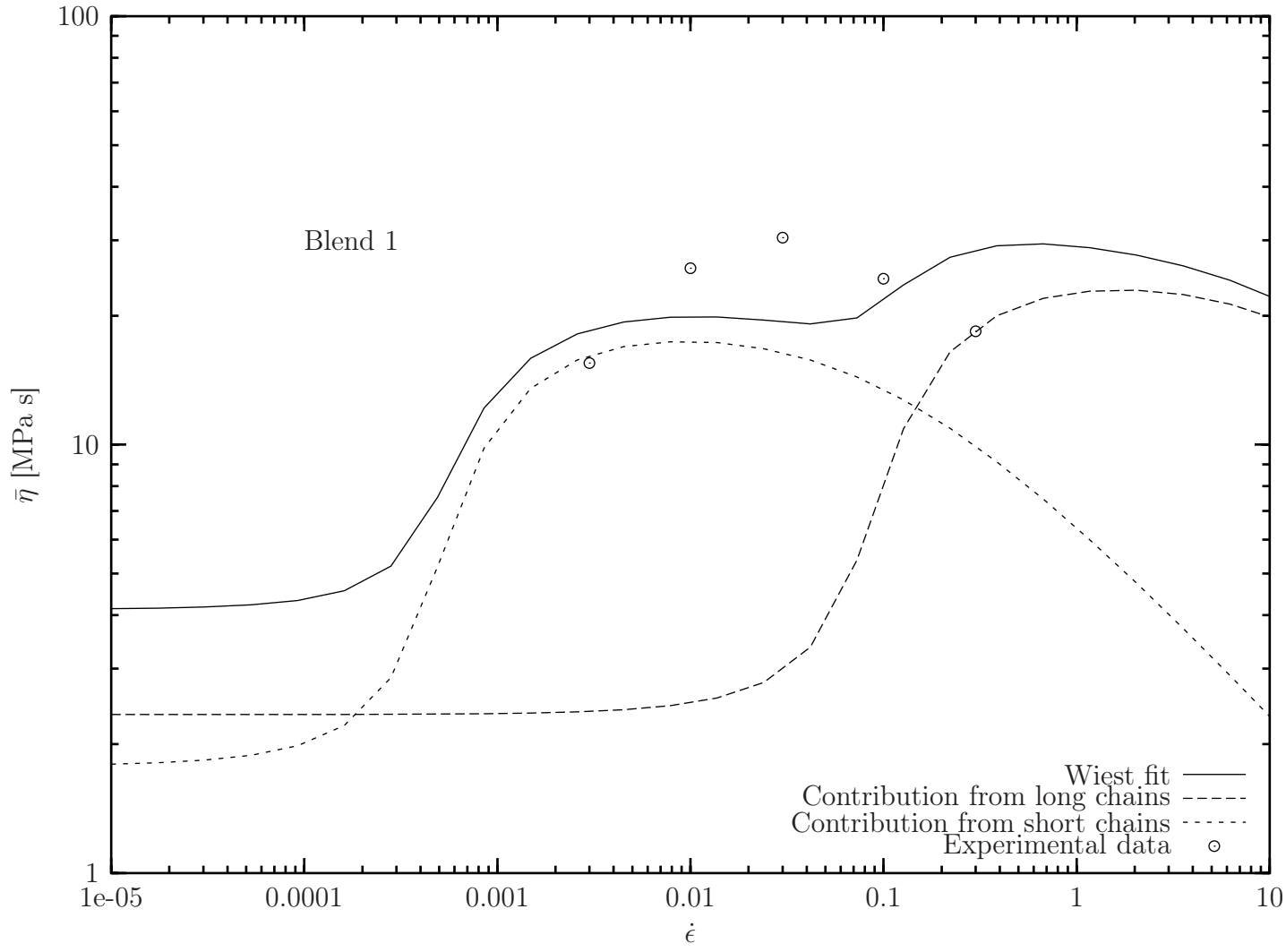
100
10
1
1e-05
0.0001
0.001
0.01
0.1
1
10
$\bar{\eta}$ [MPa s]
$\dot{\epsilon}$
Blend 1
Wiest fit
Contribution from long chains
Contribution from short chains
Experimental data

Figure 16:

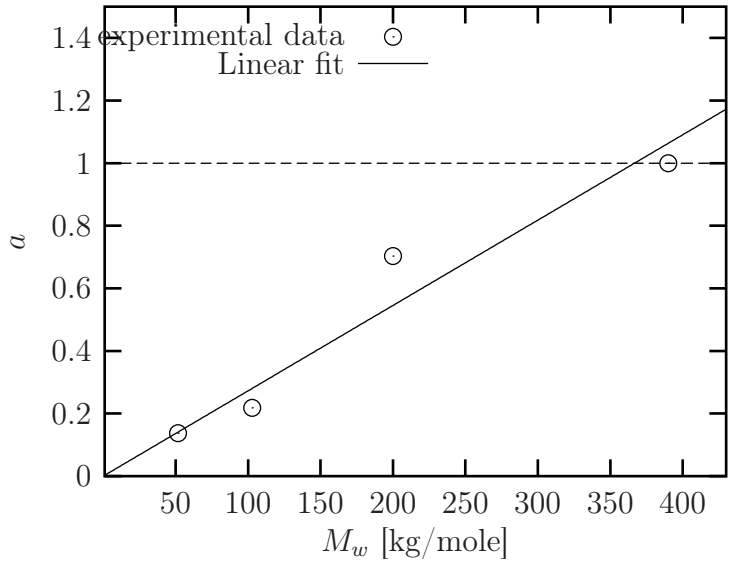
experimental data
Linear fit
1.4
1.2
1
0.8
0.6
0.4
0.2
0
a
50
100
150
200
250
300
350
400
M_w [kg/mole]

Figure 17: